International Journal of Biological Macromolecules 267 (2024) 131491

Contents lists available at ScienceDirect

International Journal of Biological Macromolecules

journal homepage: www.elsevier.com/locate/ijbiomac

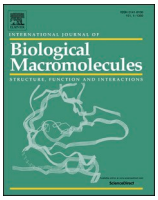

Mucoadhesive chitosan-poly (lactic-*co*-glycolic acid) nanoparticles for intranasal delivery of quetiapine – Development & characterization in physiologically relevant 3D tissue models

Dnyandev G. Gadhave [a], Mural Quadros [a], Akanksha R. Ugale [a], Mimansa Goyal [a], Seyoum Ayehunie [b], Vivek Gupta [a,*]

[a] *Department of Pharmaceutical Sciences, College of Pharmacy and Health Sciences, St. John's University, 8000 Utopia Parkway, Queens, NY 11439, USA*
[b] *MatTek Corporation, 200 Homer Ave, Ashland, MA 01721, USA*

ARTICLE INFO

Keywords:
Chitosan/PLGA nanoparticles
Intranasal delivery
Quetiapine
RPMI-2650
Monolayer
Schizophrenia
EpiNasal™

ABSTRACT

Quetiapine hemifumarate (QF) delivery to the CNS *via* conventional formulations is challenging due to poor solubility and lower oral bioavailability (9 %). Similarly, many other second-generation antipsychotics, such as olanzapine, clozapine, and paliperidone, have also shown low oral bioavailability of <50 %. Hence, the present work was intended to formulate QF-loaded biodegradable PLGA-NPs with appropriate surface charge modification through poloxamer-chitosan and investigate its targeting potential on RPMI-2650 cell lines to overcome the limitations of conventional therapies. QF-loaded poloxamer-chitosan-PLGA *in-situ* gel (QF-PLGA-ISG) was designed using emulsification and solvent evaporation techniques. Developed QF-PLGA-ISG were subjected to evaluation for particle size, PDI, zeta potential, *ex-vivo* mucoadhesion, entrapment efficiency (%EE), and drug loading, which revealed 162.2 nm, 0.124, +20.5 mV, 52.4 g, 77.5 %, and 9.7 %, respectively. Additionally, QF-PLGA formulation showed >90 % release within 12 h compared to 80 % of QF-suspension, demonstrating that the surfactant with chitosan-poloxamer polymers could sustainably release medicine across the membrane. *Ex-vivo* hemolysis study proved that developed PLGA nanoparticles did not cause any hemolysis compared to negative control. Further, *in-vitro* cellular uptake and transepithelial permeation were assessed using the RPMI-2650 nasal epithelial cell line. QF-PLGA-ISG not only improved intracellular uptake but also demonstrated a 1.5–2-fold increase in QF transport across RPMI-2650 epithelial monolayer. Further studies in the EpiNasal™ 3D nasal tissue model confirmed the safety and efficacy of the developed QF-PLGA-ISG formulation with up to a 4-fold increase in transport compared to plain QF after 4 h. Additionally, histological reports demonstrated the safety of optimized formulation. Finally, favorable outcomes of IN QF-PLGA-ISG formulation could provide a novel platform for safe and effective delivery of QF in schizophrenic patients.

1. Introduction

Schizophrenia is a complex mental condition that severely affects the patient's lifestyle, thinking, feelings, and mental abilities, leading to marked mood swings and suicidal tendencies [1,2]. With a higher rate of premature death than the general population, unfortunately, the mortality rate of the young (9–12 years) schizophrenic patient population was found to be higher than that of the general population [3,4]. Currently, available treatments for schizophrenia suffer from several limitations, including limited delivery to the brain due to the hurdle of rigid blood-brain barrier (BBB) [5–7]. Hence, higher doses (150–750 mg/day) and frequent dosing (2–3 times a day) of antipsychotics are needed to achieve therapeutic concentration in the targeted site, leading to drug-related toxicities [8].

Quetiapine hemifumarate (QF) is FDA-approved second-generation atypical antipsychotic, which is highly effective against bipolar disorders such as schizophrenia [9,10]. However, oral chronic QF administration has been associated with serious hematologic toxicities such as leukopenia and thrombocytopenia, which could occur due to metabolic conversion into highly reactive quinone-imine free radical species [11–14]. Oral bioavailability of QF is limited (approximately 9 %), when formulated in conventional immediate-release and extended-release

* Corresponding author at: College of Pharmacy and Health Sciences, St. John's University, 8000 Utopia Parkway, Queens, NY 11439, USA.
E-mail address: guptav@stjohns.edu (V. Gupta).

https://doi.org/10.1016/j.ijbiomac.2024.131491
Received 21 October 2023; Received in revised form 23 March 2024; Accepted 7 April 2024
Available online 9 April 2024

tablets [10]. Therefore, higher doses and dosing frequency are needed to maintain the drug concentration within the therapeutic window. In addition, oral QF is absorbed from the GI epithelium directly into the blood, potentially causing unwanted hematological toxicities [9]. With available formulations, QF delivery to the brain is always tricky due to the dense network of endothelial cells in the central nervous system (CNS), which acts as a biological barrier and limits the delivery of therapeutics to the brain [15,16]. Alternatively, parenteral delivery may overcome the bioavailability barrier by controlling extensive first-pass metabolism [17,18]. However, parenteral therapy seems to fail in achieving effective QF concentrations at the CNS due to the tight junction of BBB [19].

Due to above mentioned challenges, design, and development of appropriate drug delivery strategies for the site-specific, safe, and effective delivery of antipsychotic medications including QF has been of paramount importance. Currently, nose-to-brain delivery approaches have attracted the attention of researchers in CNS therapies, which provide the potential transport of therapeutics directly from the nose to brain, bypassing the BBB [3,20,21]. The drug can traverse from the nose to CNS *via* various pathways, *i.e.*, the trigeminal nerve pathway, lymphatic pathway, and majorly the olfactory pathway [16]. Intranasal (IN) delivery has been established as a proven approach for effectively delivering antipsychotics to the brain from exposed nerve endings [22]. Additionally, this strategy offers non-invasive administration and direct brain distribution by avoiding first-pass metabolism and enzymatic degradation [23]. It also aids in lowering the dose and dosing frequency, thus improving patient comfort and acceptability. Despite these advantages, IN administration has numerous limitations, such as mucociliary clearance, responsible for rapid clearance of applied formulations through the nasal cavity [24]. These nasal reflex mechanisms reduce the duration of nasal localization of applied nanoformulations, leading to diminished drug absorption *via* the nasal cavity [25]. Thereby, the inclusion of recognized gelling/mucoadhesive agents such as chitosan, poloxamer, and gellan gum in IN formulations can increase the localization time of the drug at the site of application, and help to improve the penetration in the brain [5].

According to several published reports, nanotechnology-based formulations have proven their superiority in delivering therapeutics to the brain over conventional formulations [6,26]. Several researchers reported that poly (lactic-*co*-glycolic acid) nanoparticles (PLGA-NPs) are highly suitable for drug delivery in neurological disorders because their promising features such as nanometric size (100–250 nm), acceptable biodegradability, excellent biocompatibility, controlled release ability, promising drug entrapment and loading properties [26–28]. Additionally, PLGA-NPs are an excellent carrier/vector for DNA, proteins, therapeutic agents, RNA, and vitamins. Chitosan (CH) is a natural polysaccharide, globally employed for biomedical applications due to its acceptable biocompatibility, promising safety, significant biological activity, and limited immunogenicity [20,27,29]. CH possesses special features of forming a gel in a physiological environment in the presence of mucin, which is mainly located in the nasal secretions. CH produces a protein-polysaccharide complex (electrostatic interaction) with mucin at pH 2.5 and 6.4, which is deemed responsible for mucoadhesion [30]. Further, poloxamer 407 (P407) was incorporated to prepare thermosensitive *in-situ* gels to boost the consistency and cohesiveness of the formulation [3,25]. Many researchers have utilized a combination of ionic and thermo-sensitive gelling systems for the nose-to-brain delivery of medicines, which are liquid at ambient temperature, and convert to gel at nasal cavity temperature (34 °C) [1,25].

The present work aimed to prepare QF-loaded biodegradable PLGA-NPs with appropriate surface charge modification through poloxamer-chitosan and investigate its brain-targeting and nasal epithelium transport potential in RPMI-2650 cells to overcome the limitations associated with conventional QF therapies. During the experiment, QF-loaded P407-CH-PLGA *in-situ* gel (QF-PLGA-ISG) was prepared by emulsification and solvent evaporation method. Moreover, the characterization of the QF-PLGA-NPs and QF-PLGA-ISG for particle size, polydispersity index, *ex-vivo* mucoadhesion, surface charge, *ex-vivo* hematological toxicities, accelerated stability, *in-vitro* release, *in-vitro* cytotoxicity, cellular uptake, and permeation studies were performed in RPMI-2650 cell lines to demonstrate the safety and targeting potential of the developed nanoparticles.

2. Materials and methods

2.1. Materials & cell culture

Quetiapine hemifumarate (QF) was procured from Cayman Chemical Company (Michigan, USA). Resomer® RG 502H (Poly(D, L-lactide-*co*-glycolide 50:50)) was purchased from Evonik (Piscataway, NJ, USA). Polyvinyl alcohol (PVA) was received from Sigma-Aldrich (St. Louis, MO, USA). Dichloromethane (DCM), dimethyl sulfoxide (DMSO), HPLC grade acetonitrile (ACN), 3-(4,5-dimethylthiazol-2-yl)-2,5-diphenyltetrazolium bromide (MTT), and coumarin-6 (C6) were procured from Fisher Scientific (Hampton, NH, USA). Glycol-chitosan was procured from MedChemExpress (Monmouth Junction, NJ, USA). Kolliphor$^{(R)}$ 407 was received as a gift sample from BASF Corporation (NY, USA).

Human nasal epithelial cell line (RPMI-2650) was obtained from ATCC (Manassas, VA, USA) and preserved in EMEM medium (Corning) supplemented with 10 % FBS (Atlanta Biologicals), and 1 % penicillin-streptomycin. MatTek EpiNasal™ tissues was procured as a gift sample from MatTek Life Sciences (Ashland, MA, USA) and cultured in NAS-100-MM EpiNasal™ culture medium. All cell lines and MatTek tissues were incubated at 37 °C/5 % CO_2 and 90–100 % relative humidity.

2.2. Analytical method development for QF by RP-UPLC

A reverse-phase liquid chromatography technique was developed for quantifying QF using Waters Acquity UPLC (Milford, MA, USA). The column used was XBridge® BEH Shield RP18 2.5 μm (3.0 × 100 mm). The mobile phase combined an organic phase of ACN and an aqueous phase of 0.1 % orthophosphoric acid (OPA) in a ratio of 75:25 with a flow rate of 0.3 mL/min. The wavelength used for detection was 294 nm. The data was processed using Empower 3.0 software (Waters, MA, USA).

2.3. Formulation of QF-loaded PLGA nanoparticles (QF-PLGA-NPs)

QF-loaded PLGA nanoparticles were prepared using emulsification and solvent evaporation techniques [31]. Briefly, 20 mg QF with 60 mg of PLGA was dissolved in 3 mL of organic solvent (dichloromethane) to form an organic phase, while the aqueous phase (10 mL) was composed of 1 % of polyvinyl alcohol (PVA) in deionized water. Further, QF containing organic phase was added dropwise to the aqueous phase following 4 min probe sonication with 40 % amplitude (10 s on/off cycle; Qsonica Q500, Newtown, CT, USA) to develop an O/W emulsion. This O/W emulsion was then left to evaporate overnight under moderate magnetic stirring. Simultaneously, QF-PLGA-NPs were separated from the remaining aqueous phase by centrifugation (15,000 ×*g* for 30 min), and the pellet of PLGA-NPs was then washed three times with deionized water. Finally, the developed QF-PLGA-NPs were resuspended in 1 mL of water and stored for further characterization [32].

2.4. Formulation of CH-P407-PLGA in-situ gel (ISG)

A QF-loaded *in-situ* gel formulation was developed using the appropriate and safe concentrations of mucoadhesive and *in-situ* gelling agents. Chitosan (CH) and poloxamer-407 (P407)-coated PLGA-NPs (QF-PLGA-ISG) were designed upon the addition of 2 % *w/v* CH and 18 % w/v P407 (equivalent to total formulation volume, screened through temperature-controlled magnetic stirrer) in previously developed QF-PLGA-NP suspension with continuous stirring at 300 rpm for 25 min. The CH-P407 produced a coat on the QF-PLGA-NPs. In the

current formulation, CH acted as a mucoadhesive, and P407 acted as an *in-situ* gelling agent. Further, the fabricated QF-PLGA-ISG was utilized for different studies, including globule size, viscosity, zeta potential, mucoadhesive strength, *in-vitro* release, *ex-vivo* hemolysis, *in-vitro* cytotoxicity, cellular uptake, and permeation studies.

2.5. Screening of gelation properties and concentration of polymers

Gelation properties of polymers at different concentrations and temperatures were performed using a temperature-controlled magnetic stirrer. In this context, the formulation's sol-gel transition temperature was examined and noted. Briefly, 2 mL of QF-PLGA-ISG formulations containing vials were placed on a heat-controlled magnetic stirrer. The mixture was stirred at 400 rpm with a continuous increment of 1 °C/min at a temperature. The temperature at which the stirring stopped due to sol-gel conversion was measured and noted [1,33,34].

2.6. DSC analysis

Compatibility of QF with the selected polymers (PLGA, PVA, CH, and P407) was tested utilizing DSC 6000 (PerkinElmer, Inc.; Shelton, CT, USA). Samples were analyzed at the range of 50 °C to 250 °C and the heating rate was fixed at 10 °C/min, employing an empty pan as a reference under the nitrogen purge at flow rate of 50 mL/min [16,35].

2.7. Physicochemical characterization for developed PLGA formulations

2.7.1. Particle size, polydispersity index (PDI), and surface charge (ζ-potential)

Particle size distribution of PLGA-NPs and PLGA-ISG were screened through the DLS technique utilizing Zetasizer nano ZS (Malvern Instrument, UK). Additionally, PDI was used to study the uniformity of particle size. Simultaneously, the surface charge of nanoparticle was screened by measuring the ζ-potential of the nanosystem using Zetasizer nano ZS (Malvern Instrument, UK) [36,37].

2.7.2. Analysis of entrapment efficiency and drug loading

Entrapment efficiency (%EE) and QF-loading (%DL) for developed nanoparticles were screened by measuring the quantity of free QF in a supernatant. Exactly, 1 mL of QF-PLGA-NPs and QF-PLGA-ISG formulations containing 2 mg/mL of QF (theoretical amount) were centrifuged at 15,000 rpm for 30 min. Then the supernatant was mixed with 10 mL acetonitrile. Dilutions were prepared with a 1:1 ratio of water: acetonitrile (mobile phase) and followed by QF quantification in the supernatants at 294 nm using the ultra-pressure liquid chromatography (UPLC) method. Eqs. (1) and (2) were utilized to calculate the %EE and %DL of the nanoparticles, respectively [38].

$$\%EE = \frac{\text{Weight of added drug} - \text{Weight of free drug}}{\text{Weight of entrapped drug}} \times 100 \quad (1)$$

$$\%DL = \frac{\text{Weight of entrapped drug} - \text{Weight of free drug}}{\text{Total weight of PLGA polymer and drug}} \times 100 \quad (2)$$

2.7.3. Rheological behavior of developed formulations

Rheological behavior of the QF-PLGA-NPs and QF-PLGA-ISG was assessed through a Brookfield viscometer (Brookfield Engineering Laboratories Inc., Middleboro, MA, USA), using spindle number-21. Briefly, 10 mL of sample was analyzed at the temperature of 25 °C and 34 °C. Briefly, the test speed was gradually raised from 5 to 100 rpm, and measurements were carried out in triplicates [3,39].

2.7.4. Bio-adhesion potential of developed PLGA-ISG

Consistency and cohesiveness of the developed PLGA-NPs and PLGA-ISG were evaluated using a TA.XT Plus texture analyzer (Texture Technologies Corp., Hamilton, MA, USA). In due course of experiment, the formulation was sprayed on freshly collected nasal mucosa (obtained from the animal house), and then a cylindrical probe was dipped in the formulation for 10 s. Measurements were accomplished at a velocity of 1 mm/s with a trigger force of 3 g. Simultaneously, the force needed to break the adhesion between nasal mucosa and gel was determined and reported [17,40,41].

2.7.5. In-vitro QF release

In-vitro QF release assessments were conducted utilizing the dialysis method, as reported previously [22,36]. Briefly, dialysis cassettes (0.1–0.5 mL, 2000 MWCO, Thermo Scientific, Waltham, MA, USA) were allowed to equilibrate in a previously prepared simulated nasal electrolyte solution (SNES: pH 6.4) for 10 min [42]. Then, the formulations were filtered through a syringe filter (0.22 μm), and 500 μL of each formulation was loaded into the cassette membrane. Then hydrated cassettes were immersed into a beaker containing 100 mL of SNES (pH 6.4; 34 ± 0.5 °C) using a floater while stirring at 200 rpm. 1 mL of sample was withdrawn at predefined time points, *i.e.*, 0.5, 1, 2, 4, 8, 12, and 24 h, and replenished with fresh SNES. Collected samples were then diluted with mobile phase and analyzed through the validated UPLC method, as described in Section 2.2 [43].

2.7.6. Ex-vivo hemolysis study

According to previously published reports [11,12], QF administration may induce hemolytic anemia in individuals. Therefore, it was necessary to confirm that hemolysis does not occur after IN administration. Hemolytic index <1 % is crucial to maintain RBC viability in the blood. The QF-induced hemolytic potential was analyzed using various formulations such as control (distilled water), negative control (0.01 % sodium lauryl sulfate), QF-PLGA-NPs (10, 50, and 100 μg/mL), and QF-PLGA-ISG (10, 50, and 100 μg/mL). Briefly, 4 mL of blood samples were collected through a 23-gauge needle from the lateral saphenous vein of the male Sprague Dawley rats (weighed 150 to 200 *g*); and centrifuged at 3000 rpm for 15 min to separate the cell pellet; which was then washed thrice with saline water. Later, cells were incubated with different concentrations (10, 50, and 100 μg/mL) of formulations and other control treatments at 37 °C. Finally, 200 μL samples were collected from treated cells at different time points (0.5, 4, and 10 h), followed by centrifugation for 15 min at 13,000 ×g. Eventually, absorbance for obtained samples was measured at 570 nm using a Spark 10 M Plate Reader (Tecan, Männedorf, Switzerland). Eq. (3) was used to calculate the percentage of hemolysis [44–46].

$$\text{Hemolysis Ratio}\ (\%) = \frac{Absorbance\ of\ sample - Absorbance\ of\ control}{Absorbance\ of\ negative\ control - Absorbance\ of\ control} \times 100 \quad (3)$$

2.7.7. Stability evaluation

Shelf-life or stability evaluation of fabricated QF-PLGA-NPs and QF-PLGA-ISG formulations was conducted according to ICH guidelines (Q1aR2). Formulations were kept in the stability chamber (VWR™

stability chamber, USA) for three months under prescribed accelerated stability conditions (40 °C and 75 % RH). In this context, the samples were examined for three months of crucial physicochemical parameters such as particle size, PDI, clarity, ζ-potential, and QF content [40].

2.8. Cell culture experiments

For this assay, RPMI-2650, a human nasal epithelial cell line (ATCC, Manassas, VA, USA) was grown using EMEM cell growth media augmented with 1 % antibiotics (penicillin-streptomycin) and 10 % Fetal Bovine Serum (FBS). Subsequently, cells were allowed to grow in T75 cell culture flasks (VWR, Radnor, Pennsylvania, USA) at 37 °C/5 % CO_2 until 85–90 % confluency was achieved. Confluent cells were then trypsinized and utilized for *in-vitro* cell experiments such as cell viability, cellular uptake, and cell permeability studies [38,47,48].

2.8.1. In-vitro cell viability study

This study evaluated the safety of pure QF, blank-PLGA-ISG, and QF-PLGA-ISG formulations on RPMI-2650 cell lines. Cell viability experiments were conducted utilizing MTT assay. Briefly, 2500 cells/well were seeded in TC-treated 96-well plates (VWR, Radnor, Pennsylvania, USA), followed by overnight incubation at specified conditions for adherence. The following day, cells were treated with varying concentrations of pure QF, Blank-PLGA-ISG, and QF-PLGA-ISG (equivalent to 0.78125–1000 μM of QF), and media was utilized as a control. After 24 h, the cell viability was determined by MTT assay following established protocols [49,50]. The % viability of RPMI-2650 cells was calculated by the following Eq. (4) [37].

$$\text{Cell viability } (\%) = \frac{\text{Mean absorbance of treatment}}{\text{Mean absorbance of control}} \times 100 \quad (4)$$

2.8.2. Cellular uptake by fluorescence microscopy

An established method was used to ascertain the impact of NP loading and targeting on the intracellular absorption of the encapsulated medication. Coumarin-6 (C6), 1 mg/mL, a fluorescent dye was incorporated in the formulation of NPs for cellular uptake. Briefly, RPMI-2650 cells were seeded at a density of 1×10^4 cells/well in tissue culture-treated cell imaging eight-chambered cover glass, followed by overnight incubation. The next day, cells were treated with C6-loaded PLGA and PLGA-ISG at 1 μg/mL concentration for 1 to 3 h. After incubation, cells were fixed with 4 % PFA for 10 min after each interval and rewashed twice with ice-cold PBS. Chambers were removed, and 20 μL of DAPI nuclear stain was applied dropwise to a glass slide before being covered with a cover glass. Covered glass slide kept overnight in fridge for proper staining [31]. Finally, stained slides were imaged using a fluorescence microscope (EVOS FL, Thermo Scientific, Fair Lawn, NJ, USA) [47].

2.8.3. Quantitative cellular uptake of C6 PLGA-ISG formulation

To investigate the difference in cellular uptake of C6-loaded PLGA and PLGA-ISG, we used Nexcelom Cellometer Vision (Nexcelom, Lawrence, MA, USA). The experiment was conducted after incubating C6-loaded PLGA-ISG (C6 equivalent to 1 μg/mL) with the RPMI-2650 cells (5×10^6 cells/sterile petri dish) for 3 h. The incubated cells were trypsinized and rewashed with ice-cold PBS and followed by centrifugation. Cell pellets were then distributed in 50 μL of PBS and samples were examined for C6 signals utilizing a Cellometer Vision. The mean fluorescence intensity (MFI) of C6-loaded PLGA-ISG was compared with C6 solution, and control RPMI-2650 cells [51,52].

2.8.4. Permeation across RPMI 2650 nasal epithelial cell monolayers

In the permeation experiment, RPMI-2650 cells were seeded on polyester Transwell™ inserts (12-well plates, area 0.33 cm^2, 0.4 μm pore size). Briefly, 100 μL of cell suspension was seeded at 8.5×10^4 cells/Transwell™ polyester inserts to create the air-liquid interface model, and 600 μL of media was added in the basolateral chambers to ensure monolayer growth. Finally, plates were incubated for 24 h at 37 °C, 95 % air humidity, and 5 % CO_2 [53,54].

2.8.5. Transepithelial electrical resistance (TEER)

TEER measurement was utilized to assess the integrity of the cell layer. This approach measures the ionic resistance across the cell layer throughout distinct development and differentiation stages. Using an EVOM® resistance meter and Endohm® chamber (World Precision Instruments, Sarasota, FL, USA), the TEER of RPMI-2650 cell layers was taken on every 2 to 3 days during culture to confirm the establishment of the cellular monolayer. The measurement approach comprises measuring the blank resistance (R_{Blank}) of the membrane alone (without cells) and the resistance across the cell layer on the insert membrane (R_{Total}), as the pore size and density of the insert membranes influences the TEER. Final cell membrane resistance was calculated by the following equations (Eqs. (5) and (6)) [53].

$$R_{Cells(\Omega)} = R_{Total} - R_{Blank} \quad (5)$$

$$TEER_{Cells} = R_{Cells(\Omega)} \times M_{Area(cm^2)} \quad (6)$$

2.8.6. QF permeation across RPMI-2650 cell monolayers

After 16 days with an appropriate TEER plateau values (80–85 Ω. cm^2), RPMI-2650 cells monolayer was used for the permeation study. The PLGA formulations containing QF were used to treat cells. The EMEM medium in the Transwell™ basal chamber (acceptor) was withdrawn from each well prior to the treatment and replaced with fresh media. The apical chamber (donor) of Transwell™ inserts was filled with 100 μL of 25 μM and 50 μM of QF solution; and QF-PLGA-ISG (formulations were diluted with 1× PBS, pH 7.4) and were subsequently incubated at 37 °C/5 % CO_2 and 95 % air humidity. After completion of treatment, 100 μL sample was withdrawn once/h for 3 h from the acceptor chamber and replenished with the same volume of fresh media. All permitted samples were analyzed through UV spectrophotometer for QF content in triplicate [48]. The apparent permeation coefficient (P_{app}) and steady-state flux (J_{ss}) were calculated using the equations (Eqs. (7) and (8)).

$$\text{Papp} = \left(\frac{dQ}{dt}\right) \times \left(\frac{1}{AC}\right) \quad (7)$$

$$J_{ss} = P_{app} \times C \quad (8)$$

where dQ/dt is a change in concentration/change in a time at steady state, A is the membrane surface area, and C is the initial QF concentration in the apical chamber.

2.9. Permeation of QF using EpiNasal™ 3D in-vitro nasal tissue

EpiNasal™ 3D *in-vitro* nasal tissue model (NAS-100-BETA, MatTek Corporation, Ashland, MA) was used to assess intranasal permeability of QF following nanoparticle encapsulation, following manufacturer's protocol. Briefly, the EpiNasal™ tissues were stabilized using supplied media (NAS-100-MM) in a humidified 37 °C, 5 % CO_2 incubator. Before the experiment, the integrity of EpiNasal™ tissues were screened through TEER measurement (TEER analysis conducted following 2.8.5). For the permeation study, the NAS-100-MM medium was replaced with 5 mL of prewarmed 1× PBS (to overcome protein interference). Cell culture inserts were filled with 50 μL of 1 mg/mL and 2.5 mg/mL of QF solution (control) and QF-PLGA-ISG (formulations were diluted with sterile 1× PBS, pH 7.4) and were incubated at 37 °C/5 % CO_2 and 90 ± 10 % RH. After completion of treatment, 100 μL sample was collected on 4 h and 8 h from the bottom wells. All samples were screened for QF permeation *via* validated UPLC method in triplicate. Similarly, Eqs. (7) and (8) were utilized to calculate P_{app} and J_{ss}.

2.9.1. Histopathology on MatTek EpiNasal™ tissues after 8 h of treatment

After 8 h treatments, EpiNasal™ tissues were prepared for histopathological screening. Initially, the tissues were cleaned with ethanol. The viability of EpiNasal™ tissues is essential throughout the investigation. Thus, the treated tissues were submerged in a 10 % formalin solution, significantly improving their viability. Subsequently, all tissues were stained through hematoxylin and eosin. Later, the stained tissues were placed to dry overnight and then observed under an inverted microscope at 40× magnification equipped with a color camera (Laxco, Mill Creek, WA, USA). Finally, the respective tissues were examined for damage and disruption. Structural transformations under QF formulation treated sections were investigated by comparing them against control tissues.

2.10. Data representation & statistical analysis

GraphPad Prism 9.5.1 software (Boston, MA, USA) was utilized to carry out statistical analyses. Each experiment was performed at least three times, and data were presented as means with standard deviations unless otherwise noted. Cell viability studies were performed in triplicate with $n = 6$ for each repetition. The findings were analyzed using the student's *t*-test when comparing unpaired samples from two groups. The outcomes from cytotoxicity, uptake, and permeation studies were screened through Tukey's post-hoc comparison with ANOVA. The *p*-values (*$p \leq 0.05$ or lower*) were considered statistically significant.

3. Results

3.1. Formulation and development of QF-PLGA-NPs

For QF formulation development, the appropriate biocompatible, biodegradable, and natural excipients were selected from the GRAS (Generally Recognized as Safe) approved list of polymers. As described, the choice of components for the final formulation was achieved after different trials and stability of formulations. Table 1 represents different test formulations, which were performed to investigate the proper development of QF-PLGA-NPs. As can be seen, the F5 formulation showed appropriate results compared to other test batches and was considered an optimized batch. QF-PLGA-NPs *(Batch F5)* formulation was composed of QF (20 mg), PLGA (60 mg), dichloromethane (3 mL), PVA (1 % *w/v*), tween 20 (1 % w/v), and water (10 mL), respectively

Table 1
The formulation layout for trial batches of QF-PLGA-NPs development. The development was carried out in triplicates.

Sr. no.	Formulation factors				Responses		
	Drug (mg)	PLGA (mg)	DCM (mL)	PVA (mg)	Globule size (nm)	PDI	ζ-Potential (mV)
F1	10	20	1	40	504.7 ± 11	0.61 ± 0.03	−5.31 ± 0.7
F2	20	40	2	70	282.1 ± 7.4	0.52 ± 0.02	−7.54 ± 0.4
F3	30	60	3	100	211.9 ± 9.8	0.48 ± 0.04	−14.6 ± 0.3
F4	10	40	2	70	239.8 ± 6.3	0.61 ± 0.03	−9.82 ± 0.5
F5	***20***	***60***	***3***	***100***	***154.3*** ± *1.2*	***0.12*** ± *0.01*	***−17.8*** ± ***0.6***
F6	30	20	1	40	608.9 ± 14	0.63 ± 0.03	−8.34 ± 0.7

Drug: Quetiapine hemifumarate; PLGA: Poly (lactic-co-glycolic) acid; DCM: Dichloromethane (organic phase); PVA: Polyvinyl alcohol (emulsifier).

Table 2
Final optimized composition of QF-PLGA-NPs (F5 according to trial batches) and QF-PLGA-ISG formulation (QF-PLGA-ISG formulation contained blend of 18 % *w/v* poloxamer 407 + 2 % w/v chitosan in water).

Category	Name of component	Optimized QF-PLGA-NPs composition	Optimized QF-PLGA-ISG composition
Polymer	PLGA	60 mg	60 mg
Organic solvent	DCM	3 mL	3 mL
Emulsifier	PVA	100 mg	100 mg
Aqueous phase (Q. S.)	Water	10 mL	10 mL
Natural mucoadhesive agent	Chitosan	–	200 mg
In-situ gelling agent	Poloxamer 407	–	1800 mg

Each QF-PLGA-NPs formulation contains QF 2 mg/mL, each optimized QF-PLGA-ISG formulation contains QF 2 mg/mL.

(Table 2). This composition fulfilled the appropriate requirements, such as nanometric particle size (154.3 ± 1.2 nm, surface charge (−17.8 ± 0.6 mV), PDI (0.12 ± 0.01), and %EE (75.8 ± 1.4 %) (Table 1).

3.2. Preparation of in-situ gel formulation

Many studies have suggested that numerous factors could affect the feasibility of intranasal (IN) route for delivering medications to the brain [39]. However, the IN pathway has proven more effective in delivering drugs to the brain by incorporating specific excipients (such as gelling agents, absorption enhancers, and targeting ligands) [1,55]. The current research aims to extend the residency period of the developed nanoformulation in the nasal cavity to ascertain transport the incorporated medicine to the brain. For the development of mucoadhesive formulation, various *in-situ* gelling agents were examined during the experiment. Various polymers, *i.e.*, CH, HPMC K4M, P407, and Carbopol 974P, *etc.*, were tested for their gelling properties. The flowability and gelling tendency of different concentrations of CH (1–2%*w/v*) and P407 (16–20%w/v) polymers were visually observed by temperature-controlled magnetic stirring method at ambient (25 ± 0.5 °C) and physiological temperatures (34 ± 0.5 °C). Formulation batches of 1, 2, 4, 6, 8, and 9 at 25 ± 0.5 °C represented excellent flowability, making ease of installation of the formulations at the corresponding temperature. Meanwhile, formulation batches 3, 5, and 7 demonstrated low flowability at ambient temperature, indicating difficulty in their application (Table S1). However, batches 2 and 7 were discovered to be non-flowable at 34 ± 0.5 °C due to the sol-to-gel conversion supported by its temperature modulation features. Further, batches 1, 4, 6, and 8 look flowable at physiological temperatures, and batches 3 and 5 reflect extreme hard gelation. Finally, Table S1 revealed the optimized formulation batch 7 composed with 2%*w/v* of mucoadhesive agent (CH) and 18%w/v of *in-situ* gelling agent (P407), was found to be liquid at 25 ± 0.5 °C and converted to gel at 30 ± 0.5 °C. Thus, this sol-gel transformation prevents loss or leakage from the administration site and improves IN retention time, which effectively helps to overcome nasal mucociliary clearance. The mixture of CH (2%*w/v*) and P407 (18%w/v) produced a thermosensitive gel with the appropriate consistency, whereas other concentrations made a highly rigid or highly flowable gel at a physiological temperature and pH. Furthermore, P407 and CH produced a stable gel for IN delivery at nasal temperature (34 ± 0.5 °C), unlike other polymers that made unstable gels. Hence, 2 % CH and 18 % P407 produced a better *in-situ* mucoadhesive gelling system. The detailed formulation compositions are presented in Table 2.

3.3. Investigation of QF and excipients' compatibility via DSC

DSC analysis estimated the thermal behavior and interaction

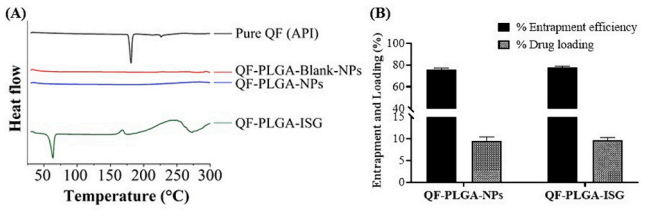

(C)

Formulations	Physicochemical Characterization		
	Particle Size (nm)	PDI	ζ-Potential (mV)
QF-PLGA-NPs	154.3 ± 1.2	0.122 ± 0.01	-17.8 ± 0.6
QF-PLGA-ISG	162.2 ± 1.4	0.124 ± 0.02	+20.5 ± 0.7

QF-PLGA-NPs: *QF-loaded PLGA Nanoparticles*; QF-PLGA-ISG: *Chitosan and poloxamer-407-loaded PLGA-NPs*; PDI: *Polydispersity index*; ζ-Potential: *Zeta potential*

Fig. 1. (A) DSC thermograms for pure QF, blank physical mixture, QF-PLGA-NPs and QF-PLGA-ISG, physicochemical characterization of developed nanoformulations: (B) particle size, PDI and ζ-potential of QF-PLGA-NPs, and QF-PLGA-ISG. (C) Analysis of QF % entrapment efficiency in QF-PLGA-NPs and QF-PLGA-ISG. Values are depicted as the mean ± SD ($n = 3$), *$p < 0.05$ corresponding to QF-PLGA-NPs formulations.

between QF and polymers. Fig. 1A shows DSC thermograms for pure QF, QF-PLGA-ISG, QF-PLGA-NPs, and blank physical mixture. Pure QF sample reflected a melting endothermic peak at 176.9 °C, which disappeared from QF-PLGA-ISG, QF-PLGA-NPs, and blank excipients mixture (Fig. 1A). Thus, the DSC findings depicted the complete encapsulation of QF in the PLGA nanoparticles. No interaction between the drug and polymer was observed, and the results indicated that the developed formulation was stable.

3.4. Physicochemical characterization of formulations

3.4.1. Particle size, pdi and ζ-potential

The dispersed particles in the prepared QF-PLGA-NPs and QF-PLGA-ISG system revealed an average particle size of154.3 ± 1.2 nm and 162.2 ± 1.4 nm (Fig. 1C), respectively. The nanodroplets of the developed PLGA should have a higher surface area, thus possessing the potential to bypass BBB *via* the IN route to efficiently deliver the therapeutics into the CNS. Moreover, the PDI for developed nanoformulations was 0.122 ± 0.01 and 0.124 ± 0.02 for QF-PLGA-NPs and QF-PLGA-ISG, respectively (Fig. 1C), which conformed mono/uniform distribution of NPs. A relatively monodispersed formulation may help in improving the stability by reducing the particle's agglomerations. Potential differences between the statistical double layer of developed PLGA-NPs and the aqueous phase were revealed −17.8 ± 0.6 mV and + 20.5 ± 0.7 mV (Fig. 1C), respectively. Additionally, representative graphs for particle size and ζ-potential are shown in Fig. S1A–D. The negative surface charge helps to increase the stability of uncoated PLGA nanoparticles due to repulsion of like-charged particles and thus, may reduce the possibility of particle aggregation [51]. Whereas the PLGA-ISG formulation possesses a positive charge, revealed by the coating of cationic polymers (CH-P04) on PLGA-NPs. It was hypothesized that the ionic interaction between the positive charge of the PLGA-ISG and the carboxy group on mucin helps to improve the mucoadhesion of the nanoparticles.

3.4.2. Drug encapsulation efficiency of PLGA nanoformulations

Drug entrapment efficiency is among the most crucial factors in determining the drug holding potential at the selected surfactant and co-surfactant concentrations. Fig. 1B represents the Drug entrapment efficiency of the generated PLGA nanoparticles. QF-PLGA-NPs and QF-PLGA-ISG nanoparticles demonstrated drug encapsulation efficiencies of 75.8 ± 1.4 % and 77.5 ± 1.6 %, respectively, resulting in a drug concentration of 1.5 ± 0.03 mg/mL and 1.6 ± 0.02 mg/mL, which was equivalent to 9.5 ± 0.9 % and 9.7 ± 0.6 % QF loading, respectively (Fig. 1B). Excellent drug encapsulation of QF in PLGA nanoparticles proved its compatibility with selected PLGA and PVA concentrations for nanoparticle synthesis, which makes them suitable carriers for QF delivery to the brain.

3.4.3. Rheological behavior of PLGA nanoparticles

Rheological behavior is vital in determining the fluidity of formulations for IN administration. If the formulation is highly viscous at room temperature, it will be challenging to administer into the nasal cavity;

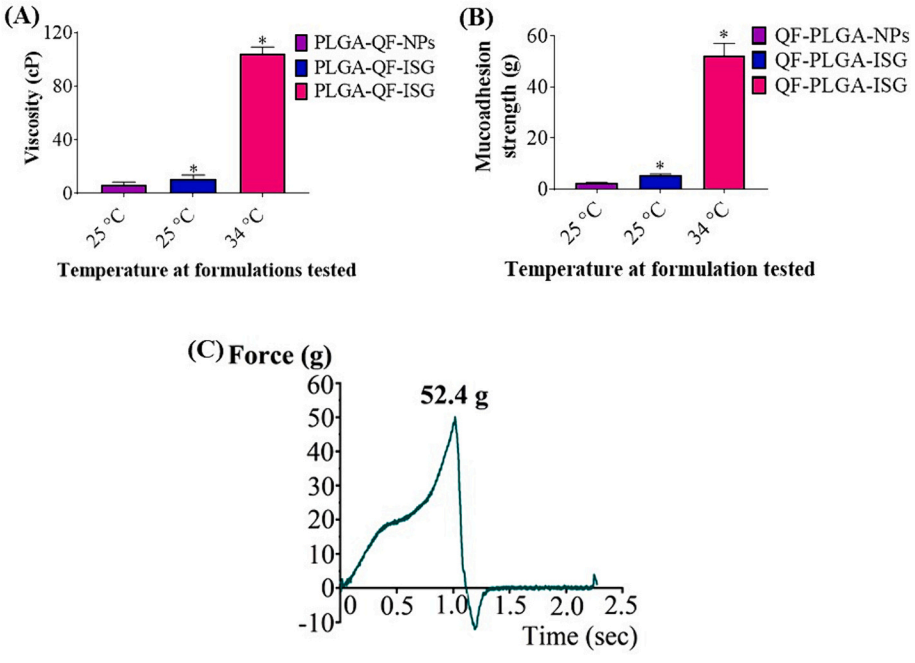

Fig. 2. (A) Determination of viscosity, (B) representative image for bio-adhesion strength and (C) *ex-vivo* bio-adhesive force of QF-PLGA-NPs and QF-PLGA-ISG formulations. Values are depicted as the mean ± SD ($n = 3$), *$p < 0.05$ corresponding to QF-PLGA-NPS formulation.

therefore, the fluidity of the formulation at ambient temperature is critical. As can be seen in Fig. 2, the QF-PLGA-NPs formulation exhibited lower viscosity (6.5 ± 0.3 cP), which indicated excellent fluidity and ease of nasal administration, which may be due to the lack of mucoadhesive and gelling polymers (Fig. 2A). At 25 °C, the viscosity for QF-PLGA-ISG (10.8 ± 0.6 cP) was revealed to be significantly less (*$p < 0.05$) that could be due to ambient temperature. However, following exposure to physiological temperature (34 °C), the viscosity of QF-PLGA-ISG was improved up to 104.1 ± 1.2 cP (Fig. 2A). Findings indicated that the CH-P407 polymers will improve the viscosity of QF-PLGA-ISG following IN administration; and hence will enable the gel to overcome the barrier of mucociliary clearance.

3.4.4. Ex-vivo bio-adhesion potential

Mucociliary clearance is the primary defense mechanism of the respiratory system, which protects the nasal cavity from external threats/infections [56]. As a result, following application, the liquid formulations are quickly washed out from the nostril. However, inadequate residence time is the foremost hurdle for the absorption of therapeutics through IN route. As seen in Fig. 2B, The QF-PLGA-NPs formulation exhibited a significantly low mucoadhesive strength (2.5 ± 0.1 g). At ambient temperature (25 ± 0.5 °C), the QF-PLGA-ISG formulation also demonstrated a low mucoadhesive force of 5.6 ± 0.4 g, which reflects more fluidity and less viscosity. However, at a physiological temperature of 34 ± 0.5 °C, a high mucoadhesive strength of 52.4 ± 4.7 g was obtained for QF-PLGA-ISG, which is reflective of *in-situ* gelling extending the local residence time (Fig. 2B). As a result, the gel formulation will remain at the absorption site for an extended time. Fig. 2C demonstrates a representative histogram of mucoadhesive strength measurements for QF-PLGA-ISG. These results show that developed QF-PLGA-ISG might help overcome the limitations associated with mucociliary clearance and improve the residence and hence transport of the entrapped drug to the intended site of action.

3.4.5. In-vitro QF release

This study helps to explore the QF release pattern from fabricated PLGA nanoformulations. Fig. 3A presents the release pattern from QF-PLGA-NP and QF-PLGA-ISG in comparison of QF suspension, in simulated nasal fluid. As can be seen, both QF-PLGA-NP and QF-PLGA-ISG demonstrated complete drug release by 24 h, with the majority of QF being released within 8 h; 97.7 ± 1.2 % from QF-PLGA-NPs and 85.7 ± 5.8 % from QF-PLGA-ISG. In comparison, QF-Suspension only demonstrated a drug release of 67.6 ± 3.4 % in 8 h (Fig. 3A), which may be attributed to low aqueous solubility of QF. The experimental results of this investigation demonstrated that the QF-PLGA-NPs released more rapidly than the QF-PLGA-ISG. It could be because the QF-PLGA-ISG formulation contained polymers, which results in a sustained release profile. The relatively faster release of QF from QF-PLGA-NPs might be due to the improved surface area of nanoformulation, which penetrates quickly *via* the dialysis membranes. It was also discovered that the droplet size of QF-PLGA-NPs and QF-PLGA-ISG was <165 nm, which helps to improve QF's solubility. Additionally, insufficient solubility of QF in QF-Suspension may cause partial drug release, where the coarse suspension particles slow down the rate of QF release *via* the dialysis cassette's pores. The zero-order model was chosen as the best-fit model because it showed the most significant regression coefficient (R^2) of 0.976 and 0.986 for the QF-PLGA-NPs and QF-PLGA-ISG, respectively (Fig. 3B). The plotted release kinetic models for QF-PLGA-NPs and QF-PLGA-ISG formulations are depicted in Fig. S2. Additionally, zero-order kinetics show continuous QF release irrespective of SNES fluid concentration until the system is saturated. At this point, it enters a linear elimination phase. According to the release study, QF-PLGA-ISG exhibited a better sustained-release impact within 24 h than QF-PLGA-NPs and QF-Suspension. In contrast, the sustained release of QF from the QF-PLGA-ISG is beneficial for extended absorption *via* IN route compared to other formulations.

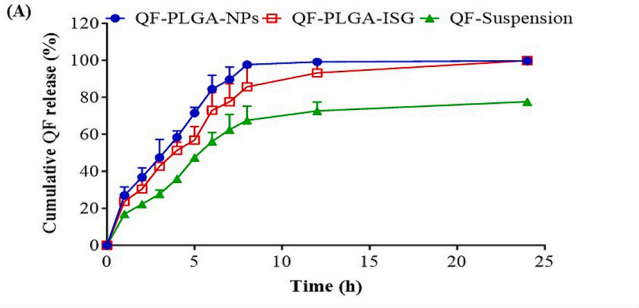

(B)

Release kinetic models	Formulations		
	QF-PLGA-NPs (R^2)	QF-PLGA-ISG (R^2)	QF-Suspension (R^2)
Zero-order	0.976	0.986	0.972
First-order	0.944	0.956	0.969
Higuchi	0.967	0.965	0.935
Hixon-Crowel cube root	0.974	0.971	0.976
Korsmeyer-Peppas	0.905	0.897	0.888
n = Release exponent	(n = 0.610)	(n = 0.589)	(n = 0.517)

QF-PLGA-NPs: *QF-loaded PLGA Nanoparticles*; QF-PLGA-ISG: *Chitosan and poloxamer-407-loaded PLGA-NPs*; R^2: *Regression coefficient*

Fig. 3. (A) Cumulative QF release from QF-Suspension, QF-PLGA-NPs and QF-PLGA-ISG over 24 h *via* a dialysis cassette. (B) The regression coefficient of kinetic models observed for QF-loaded nanoformulations.

3.4.6. Ex-vivo hemolysis study

This investigation evaluates the amount of hemoglobin released after erythrocyte destruction by QF-PLGA formulations. Due to the production of minimal oxyhemoglobin, QF-PLGA-NPs and QF-PLGA-ISG nanoparticles in the study demonstrated decreased rates of RBC hemolysis compared to 0.01 % of SLS and QF-Suspension. Furthermore, compared to QF-Suspension and QF-PLGA-NPs, the QF-PLGA-ISG nanoparticles had much-reduced hemolysis (<3.5 %) after 10 h of treatment at a higher concentration (100 μg/mL). This is due to the protective effect of CH-P407 coating the nanoparticles' surface, which lowers the oxidative stress caused by QF and exhibits protective effects on erythrocytes (Fig. 4A and B). Findings suggested that all QF-loaded NPs have considerably less potential to induce hemolysis than 0.01 % SLS (negative control) and plain QF-Suspension. As reported previously

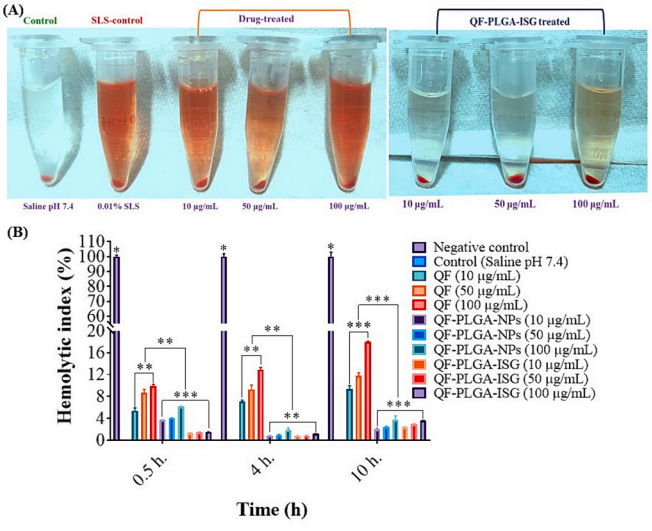

Fig. 4. (A) Visual examination of the blood samples treated with 10, 50 and 100 μg/mL of pure QF, QF-PLGA-NPs and QF-PLGA-ISG formulation against 0.01 % of negative control (SLS) in the microcentrifuge tubes and (B) % hemolysis (hemolytic index) caused by pure QF, QF-PLGA-NPs and QF-PLGA-ISG at different concentrations (10, 50 and 100 μg/mL) against negative control. Data expressed as mean ± SD ($n = 3$). *$p < 0.05$, **$p < 0.01$, ***$p < 0.001$.

Table 3
Stability evaluation of QF-PLGA-NPs and QF-PLGA-ISG after 3 months.

Formulations	Parameters	Time			
		Initial	1 month	2 months	3 months
QF-PLGA-NPs	Particle size* (nm)	154.3 ± 1.2	167.8 ± 1.6	168.5 ± 2.4	172.4 ± 2.6
QF-PLGA-ISG		162.2 ± 1.4	176.4 ± 1.9	178.2 ± 1.3	175.5 ± 2.8
QF-PLGA-NPs	Polydispersity index*	0.122 ± 0.01	0.242 ± 0.05	0.268 ± 0.03	0.231 ± 0.02
QF-PLGA-ISG		0.124 ± 0.02	0.264 ± 0.08	0.228 ± 0.05	0.262 ± 0.03
QF-PLGA-NPs	Zeta potential* (mV)	−17.8 ± 0.6	−19.2 ± 1.1	−17.6 ± 0.8	−17.7 ± 0.7
QF-PLGA-ISG		+20.5 ± 0.7	+19.8 ± 0.9	+19.6 ± 1.6	+19.2 ± 1.2
QF-PLGA-NPs	Entrapment efficiency* (%)	75.8 ± 1.4	75.7 ± 0.8	75.8 ± 2.6	75.3 ± 1.4
QF-PLGA-ISG		77.5 ± 1.6	77.5 ± 1.3	77.5 ± 2.2	76.9 ± 1.9

[11], this investigation was primarily concerned with hemolytic evidence of QF, such as leukopenia, neutropenia, thrombocytopenia, and hemolytic anemia. Ultimately, the results demonstrated the QF-loaded biodegradable PLGA formulation to be biocompatible with blood samples, which can diminish the hemolytic potential of QF.

3.4.7. Stability evaluation

An accelerated stability assay was conducted as per ICH guidelines for up to 3 months, and selected formulations were assessed for particle size, PDI, clarity, ζ-potential, and QF content. All the evaluation parameters were observed to be within the accepted limits; thus, there was no significant variation in the test results and no signs of instability (Table 3). Therefore, optimized QF-PLGA-NPs and QF-PLGA-ISG formulations retained excellent stability.

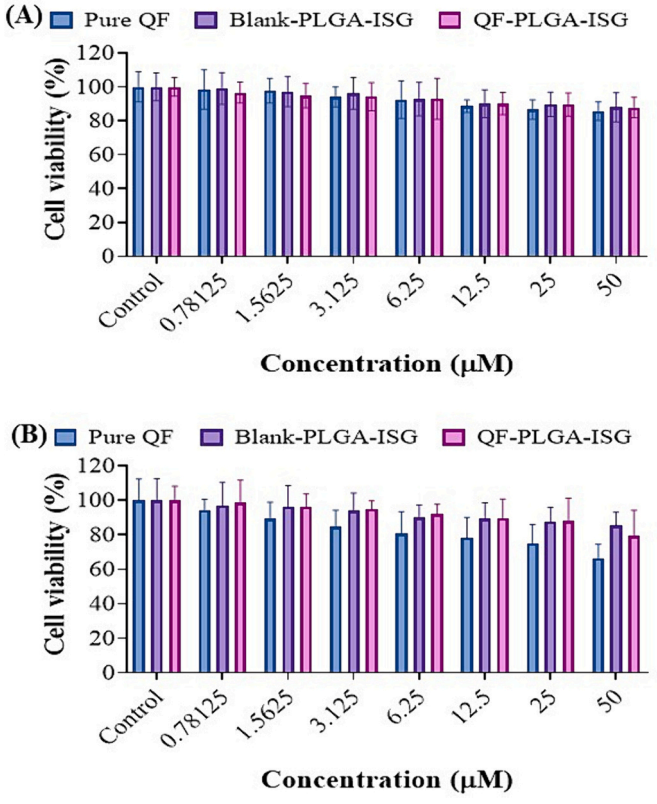

Fig. 5. MTT assay and cell viability comparison for pure QF, blank PLGA-ISG and QF-PLGA-ISG formulations on human nasal epithelial RPMI-2650 for (A) 12 h and (B) 24 h of treatments. All values are expressed as mean ± SD ($n = 3$), $^*p < 0.05$.

3.5. Cell culture experiments

3.5.1. In-vitro cytotoxicity

The *in-vitro* cell viability analysis was conducted to determine the safety of the developed QF-PLGA-ISG formulation on human nasal epithelial cell line RPMI-2650. As can be seen in Fig. 5, The safety of QF was enhanced using biodegradable cationic PLGA nanoparticles, and no significant cytotoxicity was not observed after treatment with higher concentrations of up to 50 μM of the QF-PLGA-ISG formulation. Cytotoxicity, after 12 and 24 h of treatment with developed nanoformulations is shown in Fig. 5. Both blank and QF-loaded PLGA-ISG, along with plain QF demonstrated ≈90 % cell viability at the highest concentration of 50 μM after 12-hour treatment (Fig. 5A). However, plain QF (50 μM) demonstrated significant toxicity after 24-hour exposure, demonstrated by 66.2 ± 3.0 % cell viability, which was circumvented by encapsulation in PLGA-ISG (79.4 ± 3.3 %) (Fig. 5B). Blank PLGA-ISG demonstrated 85.2 ± 4.7 % cell viability, thus confirming safety of formulation excipients. In addition, cytotoxicity results for 4 h treatment with nanoformulations are illustrated in Fig. S3. 4 h cytotoxicity was proposed to demonstrate the safety of the formulation for permeation studies. Findings concluded that the developed PLGA NPs did not cause cytotoxicity at higher concentrations (90–95 % cell viability up to 50 μM) (Fig. S3). Hence, the developed formulation was deemed safe for nasal epithelial cell lines.

3.5.2. Qualitative in-vitro cellular uptake of PLGA-ISG by fluorescence microscopy

Fluorescence-loaded C6-PLGA-ISG was fabricated to detect the uptake of optimized formulation in the intracellular environment. C6 (dye) is generally released very slowly; therefore, the work aims to improve

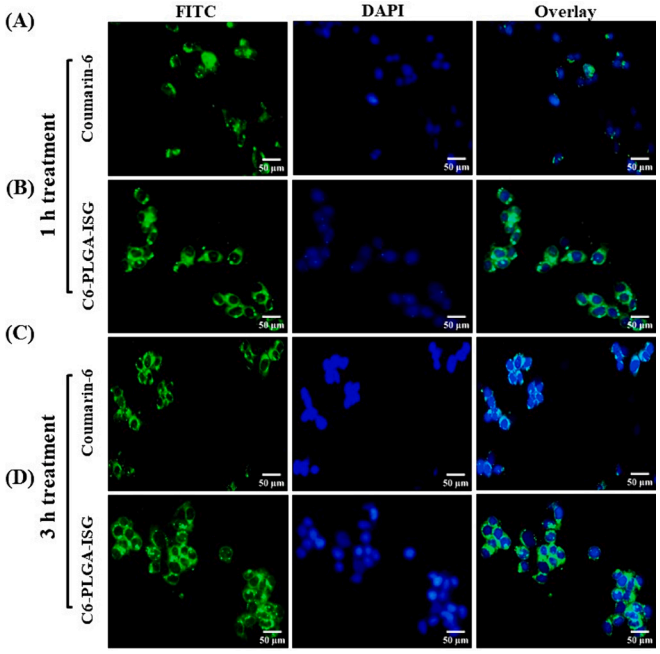

Fig. 6. *In-vitro* cellular uptake of C6 (control) and C6-PLGA-ISG in RPMI-2650 cells. Fluorescence microscopy images: (A) control treated cells for 1 h (Nuclei are stained blue with DAPI and C6/C6-loaded-PLGA are stained green), (B) C6-PLGA-ISG treated cells for 1 h, (C) control treated cells for 3 h and (D) C6-PLGA-ISG treated cells for 3 h. Scale bar = 50 μm. (For interpretation of the references to color in this figure legend, the reader is referred to the web version of this article.)

the release and uptake of the dye into the cells. Cellular uptake studies depict intact nanoparticle uptake by cells in an aqueous extracellular environment. Fig. 6 shows qualitative fluorescence illustrations of RPMI-2650 cells incorporated with C6-loaded nanoparticles for 1 (Fig. 6A & B) and 3 h, (Fig. 6C & D) respectively. According to observations, it was confirmed that C6-loaded PLGA-ISG exhibited higher uptake compared to the control (plain C6 solution). It was also demonstrated that C6-PLGA-ISG localized in the cells for a longer time with excessive fluorescence intensity, observed after 3 h of incubation. The findings assure the maximum uptake of CH-P407-coated cationic particles, thus highlighting the controlled release potential of polymeric NPS in cellular environments.

3.5.3. Quantitative in-vitro cellular uptake

A fluorescence intensity quantification experiment was performed after incubating the cells with C6-PLGA-ISG for 3 h, to learn more about the impact of PLGA-ISG on intracellular uptake of encapsulated drug molecules. As represented in Fig. 7A, C6-loaded PLGA-ISG demonstrated about twice the fluorescence intensity compared to plain C6 control (Fig. 7A & C). Fig. 7B demonstrates representative fluorescent count of cells, for GFP intensity (Fig. 7B). Fig. S4 depicted quantitative presentation of *in-vitro* cellular uptake for different treatments such as control, C6 solution and C6-PLGA-ISG by Nexcelom Cellometer Vision. Quantification of the green protein fluorescence (GFP) intensity is represented in Fig. 7C, demonstrating 95.2 ± 4.6 % cells with GFP signal for C6-PLGA-ISG, which was statistically significant *(*p ≤ 0.05)* when compared to 76.3 ± 3.9 % cells with plain C6 treatment, and only 0.15 ± 0.02 % for control untreated RPMI2650 cells (Fig. 7C). Outcomes reflect that the C6-PLGS-ISG formulation treated cells exhibit 7387.2 ± 320 fluorescence intensity, which was superior to 3991.8 ± 184 and 1212.7 ± 64 fluorescence intensities of C6 solution and control treated cell lines, respectively. The interaction between the anionic surface of the cellular membrane and the cationic charge of PLGA-ISG facilitates the easy absorption of the nanoparticles into the cells. Hence, CH-P407, as cationic polymers, make cellular uptake easier. As a result, the C6-PLGA-ISG formulation with a higher positive charge *(+20.5 mV)* exhibited a superior uptake profile.

3.5.4. QF permeation across RPMI-2650 cell monolayers

The RPMI2650 human nasal epithelial cell monolayer was evaluated for intranasal permeation of QF after encapsulation in the optimized

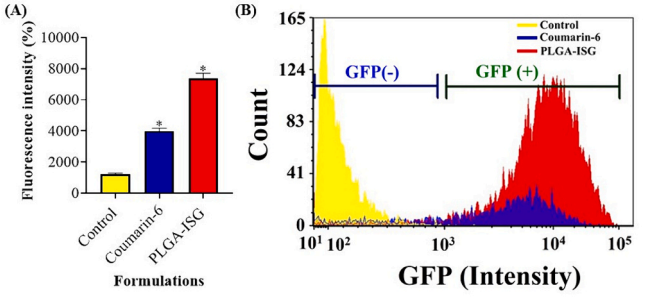

(C)

Sr. No.	Formulation	Green fluorescence protein % of cells (+)	Fluorescence intensity geometric mean
1	Control RPMI-2650 cells	0.15 ± 0.02	1212.7 ± 64
2	C6 solution	76.3 ± 3.9	3991.8 ± 184
3	C6-PLGA-ISG	95.2 ± 4.6	7387.2 ± 320

RPMI-2650: *RPMI-2650 nasal epithelial cell lines*; C6:*Coumarin-6*; C6-PLGA-ISG: *Coumarin-6-loaded PLGA-ISG*

Fig. 7. (A) Quantitative presentation of fluorescence intensities by Nexcelom Cellometer Vision and (B) internalization of fluorescence and its intensity in RPMI0-2650 cells and (C) findings from Nexcelom Cellometer analysis based on fluorescence intensity for control RPMI-2650 cells, C6 solution and C6-PLGA-ISG. Data expressed as mean ± SD ($n = 3$) *$p < 0.05$.

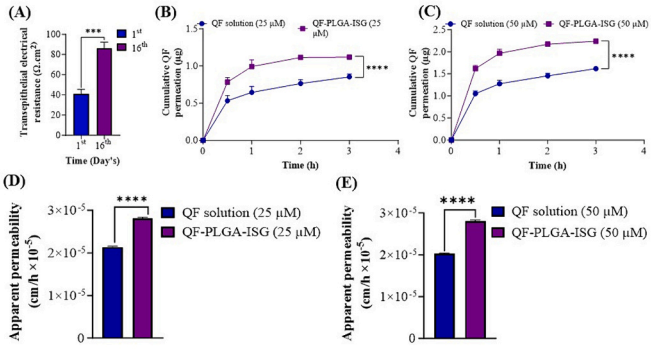

(F)

Formulation	Flux J_{ss} (µg/cm²/h)	Permeability coefficient P_{app} (cm/h × 10^{-5})	Cumulative QF permeated at 3 h (µg)
QF Solution (25 µM)	2.35 ± 0.2	2.13 ± 0.1	0.85 ± 0.03
QF-PLGA-ISG (25 µM)	3.08 ± 0.4	2.80 ± 0.2	1.12 ± 0.03
QF Solution (50 µM)	4.54 ± 0.3	2.02 ± 0.3	1.61 ± 0.04
QF-PLGA-ISG (50 µM)	6.28 ± 0.5	2.80 ± 0.4	2.24 ± 0.04

QF-Solution: *Quetiapine hemifumarate solution*; QF-PLGA-ISG: *Chitosan and poloxamer-407-loaded PLGA-NPs*; J_{ss}: *Steady state flux*; P_{app}: *Apparent permeability*

Fig. 8. (A) Transepithelial electrical resistance (TEER) value for RPMI-2650 monolayer on Transwell™ after 1st and 16th day of incubation. Cumulative amount of QF permeated across the RPMI-2650 epithelial cell line incubated on Transwell™ inserts after 3 h treatment from (B) 25 and (C) 50 µM of QF solution and QF-PLGA-ISG. Apparent permeability of (D) 25 and (E) 50 µM QF solution and QF-PLGA-ISG and (F) Permeation results of QF, permeated across the nasal epithelial cells RPMI-2650 (concentration of QF in donor chamber, *Cd* = 1.1 and 2.2 µg/mL and volume of NPs in donor compartment, *Vd* = 100 µL). Data expressed as mean ± SD ($n = 3$). **$p < 0.01$, ***$p < 0.005$ and ****$p < 0.001$.

PLGA-ISG. To develop a monolayer, RPMI-2650 cells were cultured on transwell inserts for 14 days to encourage the development of a cellular monolayer tissue. Transepithelial resistance (TEER) was tested every 2–3 days until a plateau in TEER values was achieved (Day 16). On day 16, TEER values were measured to be 86.4 Ω.cm^2, compared to 41.2 Ω.cm^2 on day 1 (Fig. 8A). Results of cumulative QF transport from 25 µM and 50 µM QF-PLGA-ISG transport across RPMI-2650 cell monolayers are shown in Fig. 8B and C, respectively. As can be seen, following a 3 h incubation period, 1.1 ± 0.02 µg and 2.2 ± 0.01 µg of QF permeated from 25 and 50 µM of QF-PLGA-ISG, which is significant higher (****$P < 0.001$), compared to 0.86 ± 0.05 µg and 1.6 ± 0.04 µg of QF permeated following same concentrations of plain QF solution, respectively (Fig. 8B & C). It can also be seen that the *in-situ* gelling system demonstrated rapid QF permeation than the QF solution. That is because a cationic mucoadhesive agent could enhance the nasal residence time as well as positive charge particles interacting with negative charge cell membrane. This mechanism helps in opening pores of cell membrane, hence the rapid drug permeation occurred through QF-PLGA-ISG formulation. Additionally, mucoadhesive polymers could enhance the localization time, resulting in enhanced permeation of QF through QF-PLGA-ISG formulation. Comparative assessment of the steady-state flux (J_{ss}) and permeability coefficient (P_{app}) was conducted for QF-PLGA-ISG formulations over 3 h. The QF-PLGA-ISG formulation exhibited significantly higher values for J_{ss} and Papp than other formulations (**$P < 0.01$). The 50 µM QF-PLGA-ISG demonstrated highly significant (****$p \leq 0.001$) P_{app} (2.80 ± 0.4 cm/h × 10^{-5}) and J_{ss} (6.28 ± 0.5 µg/cm^2/h) than the P_{app} (2.02 ± 0.3 cm/h × 10^{-5}) and J_{ss} (4.54 ± 0.3 µg/cm^2/h) of 50 µM QF solution after 3 h of treatment (Fig. 8D–F). These results illustrate the potential of the developed formulation, which can overcome the barrier of BBB and enhance QF penetration towards the CNS.

3.6. Permeation of QF across EpiNasal™ 3D in-vitro tissue samples

Intranasal (IN) permeation potential of optimized QF-PLGA-ISG formulation was screened across EpiNasal™ tissue samples.

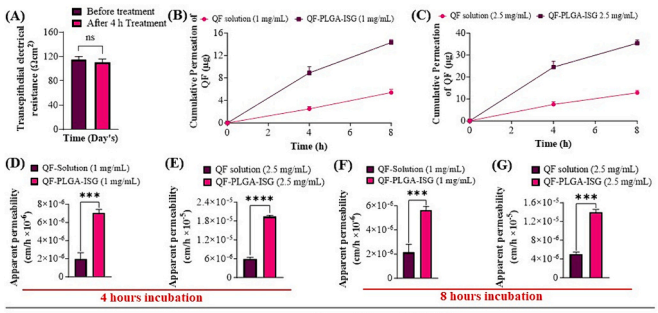

(H)

Formulations	Flux J_{ss} (µg/cm²/h)		Permeability coefficient P_{app} (cm/h × 10⁻⁵)		Cumulative QF permeated (µg)	
	After 4 h	After 8 h	After 4 h	After 8 h	After 4 h	After 8 h
QF Solution (1 mg/mL)	3.9×10^{-8}	4.2×10^{-8}	1.9×10^{-6}	2.1×10^{-6}	2.5 ± 0.3	5.4 ± 0.1
QF-PLGA-ISG (1 mg/mL)	1.4×10^{-7}	1.1×10^{-7}	7.3×10^{-6}	5.6×10^{-6}	8.9 ± 1.5	14.3 ± 0.3
QF Solution (2.5 mg/mL)	2.9×10^{-7}	2.5×10^{-7}	5.9×10^{-6}	5.0×10^{-6}	7.5 ± 0.3	12.8 ± 0.3
QF-PLGA-ISG (2.5 mg/mL)	9.6×10^{-7}	6.9×10^{-7}	1.9×10^{-5}	1.3×10^{-5}	24.5 ± 2.6	35.4 ± 0.6

QF-Solution: *Quetiapine hemifumarate solution*; QF-PLGA-ISG: *Chitosan and poloxamer-407-loaded PLGA-NPs*; J_{ss}: *Steady state flux*; P_{app}: *Apparent permeability*

Fig. 9. (A) Transepithelial electrical resistance (TEER) for MatTek EpiNasal™ tissue after initial and 4 h of treatment. The cumulative amount of QF permeated across MatTek EpiNasal™ tissue after 8 h of treatments from (B) 1 mg/mL and (C) 2.5 mg/mL of QF solution and QF-PLGA-ISG. Apparent permeability after 4 h treatment of (D) 1 mg/mL and (E) 2.5 mg/mL QF solution and QF-PLGA-ISG. Apparent permeability after 8 h treatment of (F) 1 mg/mL and (G) 2.5 mg/mL QF solution and QF-PLGA-ISG and (H) Permeation outcomes of QF, permeated across the MatTek EpiNasal™ tissue. Data expressed as mean ± SD ($n = 3$). $^{**}p < 0.01$, $^{***}p < 0.005$ and $^{****}p < 0.001$.

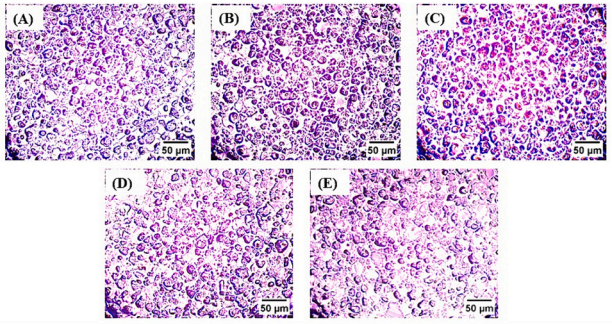

(F)

Treatment of formulations	Histopathological observations			Overall histopathology score
	Haemorrhages in EpiNasal™ tissues	Degeneration of EpiNasal™ tissues	Inflammation in EpiNasal™ tissue	
Control/saline	NAD	NAD	NAD	NAD
QF Solution (1 mg/mL)	NAD	NAD	NAD	NAD
QF-PLGA-ISG (1 mg/mL)	NAD	NAD	NAD	NAD
QF Solution (2.5 mg/mL)	NAD	Focal (+)	Focal (+)	NAD
QF-PLGA-ISG (2.5 mg/mL)	NAD	NAD	NAD	NAD

Control: *Untreated tissues*; Overall pathology score as- NAD: *No abnormalities found*; Focal (+): *Minimal changes*; Focal (++): *Mild changes*; Focal (+++): *Moderate changes*; *Focal* (++++): *Severe changes*.

Fig. 10. Histological investigation of EpiNasal™ tissue sections after 8 h treatment with QF formulations, (A) Control (Untreated tissue), (B) QF solution (1 mg/mL) treated tissues, (C) QF solution (2.5 mg/mL) treated tissues, (D) QF-PLGA-ISG (1 mg/mL) treated tissues and (E) QF-PLGA-ISG (2.5 mg/mL) treated tissues. (F) Histopathological report of control, QF solution 1 mg/mL treated, QF solution 2.5 mg/mL treated, QF-PLGA-ISG 1 mg/mL treated, and QF-PLGA-ISG 2.5 mg/mL treated EpiNasal™ tissues samples after 8 h of treatment.

Transepithelial electrical resistance (TEER) was measured before the treatment of the tissue samples. Initially, the TEER values were estimated to be 115.2 ± 4.8 Ω.cm^2, which remained consistent after 4 h of treatment (110.7 ± 5.5 Ω.cm^2) (Fig. 9A). Outcomes of cumulative QF permeation from 1 mg/mL and 2.5 mg/mL of QF-PLGA-ISG across EpiNasal™ tissues are shown in Fig. 9B and C, respectively. After 4 h treatment, 8.9 ± 1.1 µg and 24.5 ± 2.6 µg of QF permeated from 1 mg/mL and 2.5 mg/mL of QF-PLGA-ISG were found to be significantly higher ($^{**}P < 0.01$) than 2.5 ± 0.4 µg and 7.5 ± 1.2 µg of QF permeated following same concentrations of QF solution, respectively. Similarly, after 8 h treatment, 1 mg/mL and 2.5 mg/mL of QF-PLGA-ISG revealed significantly ($^{**}P < 0.01$) better permeation of 14.3 ± 0.5 µg and 35.4 ± 1.5 µg than the permeation (5.4 ± 0.6 µg and 12.8 ± 1.1 µg) of QF solution for the same concentrations (Fig. 9B & C). These outcomes demonstrated that the *in-situ* gelling approach accelerates the QF permeation rate more than the QF solution. Cationic mucoadhesive polymers may improve nasal localization time, and positively charged molecules interact with the negatively charged cell surface. This approach helps open the epithelial membrane's pores and accelerates the rate of QF permeation through the QF-PLGA-ISG formulation. Comparative examination of the steady-state flux (J_{ss}) and apparent permeability (P_{app}) was performed for QF-PLGA-ISG formulations over 4 and 8 h. The QF-PLGA-ISG demonstrated higher values for J_{ss} and P_{app} than the QF solution ($^{**}P < 0.01$). Fig. 9D and E represent higher P_{app} for QF-PLGA-ISG than the P_{app} of QF solution after 4 h of treatment. Whereas, the 1 mg/mL and 2.5 mg/mL QF-PLGA-ISG revealed very significant ($^{****}p \leq 0.001$) P_{app} (5.6×10^{-6} and 1.3×10^{-5}) and J_{ss} (1.1×10^{-7} and 6.9×10^{-7}) than the P_{app} (2.1×10^{-6} and 5.0×10^{-6}) and J_{ss} (4.2×10^{-8} and 2.5×10^{-7}) of 1 mg/mL and 2.5 mg/mL QF solution after 8 h of treatment (Fig. 9F–H). These outcomes represent the potential of the fabricated QF-PLGA-ISG, which can overcome the physiological barrier and improve QF delivery to the brain. Comparing the findings of this study with the QF permeation study across RPMI-2650 cell monolayers, both studies reproduced the results. Hence, the permeation across the RPMI-2650 monolayer has precisely correlated with the findings of permeation across EpiNasal™ tissues. These outcomes represent the potential of fabricated QF-PLGA-ISG, which can overcome the physiological barrier and improve QF delivery to the brain.

3.6.1. Histopathological screenings

Safety of developed QF-PLGA-ISG formulation was conducted in normal EpiNasal™ tissues to determine any histopathological modifications or toxicity indications after IN administration. The pathological illustrations of control, QF-PLGA-ISG, and QF-solution treated tissues after 8 h of treatment are depicted in Fig. 10A–E. As can be seen, microscopic images demonstrated no abnormal influences of optimized formulations in mucosal structures. Histological reports of Control, QF-PLGA-ISG treated, and QF solution treated tissues shown in Fig. 10F did not demonstrate any significant damage in the Control, QF-PLGA-ISG treated, and QF solution treated EpiNasal™ tissues, which confirmed the safety of optimized formulation in IN application. Simultaneously, the histological report's overall pathological score demonstrated no abnormalities in the treated tissues. Therefore, the optimized QF-PLGA-ISG formulation was found safe for IN administration.

4. Discussion

Lipophilicity and molecular weight are two significant physicochemical features of a drug that control penetration *via* the nose-to-brain pathway. QF, a suitable candidate for nose-to-brain delivery, is a practically water-insoluble medication with low molecular weight (441.5 g/mol) and appropriate lipophilicity (log $p = 2.8$) [9]. Associated limitations of conventional QF dosage forms include rapid first-pass metabolism, short $t_{1/2}$, lower bioavailability of QF, and hematological side effects [57].

The current investigation demonstrated the potential to address these limitations of available treatments with QF. In the present work, QF has been reformulated using biodegradable and biocompatible PLGA nanoparticles through scalable emulsification and solvent evaporation techniques [32]. Despite the nasal route advances in brain delivery, it is linked with different limitations like mucociliary clearance (defensive mechanism of the respiratory system) and losing dose, even unsuitable for liquid formulations. Hence, the nasal clearance barrier has been addressed by converting the QF-PLGA-NPs into *in-situ* gel with the help of biodegradable cationic polymer CH and *in-situ* gelling agent P407,

using the cold method [35]. Moreover, the developed QF-PLGA-NPs were further evaluated for their physiochemical properties, *in-vitro release*, and cell cycle experiments.

Optimized QF-PLGA-NPs and QF-PLGA-ISG reproduced nanometric particle sizes, the findings have precisely complied with the results of previously reported studies [58]. Particle size is a crucial parameter that helps to improve the drug permeation across the nasal mucosa and successfully targets the QF towards the site of action. Simultaneously, QF-PLGA-NPs and QF-PLGA-ISG revealed an optimum PDI, demonstrating uniform size distribution of nanosized particles. Uniform PDI helped in calculating the average monodispersity of nanoparticles. ζ-Potential experiments demonstrated the stability of developed nanoparticles, wherein formulated QF-PLGA-NPs depicted negative surface charge, which helps to increase the stability of uncoated PLGA nanoparticles, which could be due to the repulsion of like-charged particles and consequently reduce the probability of particle aggregation. Simultaneously, the PLGA-ISG formulation exhibited a positive surface charge, which could be due to the coating of cationic polymers (CH-P04) on QF-PLGA-NPs. It was hypothesized that the ionic interaction between the positive charge of PLGA-ISG and the carboxy group on mucin helps to improve the mucoadhesion of the nanoparticles. Chatzitaki et al., 2020, developed chitosan-coated PLGA-NPs for brain delivery and revealed a cationic surface charge that complies with the findings of QF-PLGA-ISG formulation [40].

Optimized QF formulations exhibited superior drug entrapment, which confirmed the loading potential of optimized formulations. The maximum amount of drug is entrapped within PLGA nanoparticle core, which may improve QF solubility, provide protection against enzymatic degradation, improve stability and absorption. Viscosity is essential in determining the fluidity of IN formulations for the feasibility of administration [59]. The highly viscous formulation is challenging to administer in the nose. Therefore, formulation fluidity at ambient temperature is mandatory. The developed QF-PLGA-ISG revealed excellent fluidity at room temperature, but it turns to gel at physiological temperature. Because polymer P407 does not change its transition at room temperature, but it rapidly converts to the gel once the temperature increases.

Similarly, the mucoadhesive strength of formulation is crucial to overcome the nasal clearance barrier. Mucociliary clearance is an ideal characteristic of the nasal mucosa/respiratory system (a nasal defensive mechanism), which clears the formulation from the application site. However, more localization time is needed to absorb therapeutics through the IN route [60]. Developed QF-PLGA-ISG contains CH-P407 cationic-charged polymers. The P407 converts to gel at nasal temperature; however, CH makes a strong adhesive bond with nasal mucosa when it encounters mucin. The formulation remains in the nose longer, and the QF can be released sustainably. The findings demonstrated that QF-PLGA-ISG exhibited excellent mucoadhesive potential, efficiently addressing the mucociliary clearance limitation [22].

In-vitro release from optimized formulations is essential for predicting the formulation's *in-vivo fate and* the therapeutic outcomes. This screening helped determine *in-vitro and in-vivo* correlation for the developed formulation. The QF-PLGA-NPs and QF-PLGA-ISG showed a biphasic release pattern exhibited by an initial burst release due to the particle surface coat dissolution. Which may be due to diffusion of the drug from the carrier when in contact with the nasal fluid. Subsequently, a sustained release pattern was followed that may be attributed to the diffusion of QF through the matrix or the gradual erosion of PLGA. The published work [61] observed a similar release mechanism for PLGA nanoparticles, which complies with experimental findings. The sustained release potential of developed formulation allows for prolonging drug uptake to the brain, which helps to reduce dose and dosing frequency along with limitations of conventional formulation. For a better understanding of the release mechanism of QF from the QF-PLGA-ISG, different release models were utilized for the *in-vitro* release data, and the zero-order kinetic model was found to be the best-fitting model. This model represents the constant QF release from the PLGA core and may enhance therapeutic impact by reducing the adverse effects. This model mainly represents the sustained/controlled release of QF from the developed PLGA formulations [2].

Hemolysis is a complex event in which red blood cells (RBCs) burst and disintegrate. No alternative approach is available currently to detect hemolysis except the *ex-vivo* methods. This study estimated the amount of hemoglobin released following erythrocyte destruction to assess the hemolytic impact of developed QF-PLGA formulations [62]. Outcomes of the hemolysis demonstrated that all QF-loaded formulations have a considerably lower possibility to induce hemolysis than the negative control and QF-Suspension. Some previous investigations mainly involved hemolytic evidence of QF, like neutropenia, leukopenia, hemolytic anemia, and thrombocytopenia [63]. Eventually, the results indicated the QF-loaded biodegradable PLGA formulations are highly compatible with physiological samples. The PLGA nanoparticles are reported [64] for their biodegradability and biocompatibility, making them non-toxic and safer. PLGA tends to be released sustainably, which further helps to protect the blood from direct exposure to QF and degradation of RBCs. These vital properties of PLGA make it safe and valuable for QF delivery compared to other dosage forms.

Another standard for successfully developing a delivery system is the stability and shelf-life of the formulation. The objective of stability testing is to establish the shelf life as well as the suggested storage conditions for the drug product, as well as to provide evidence regarding how the quality and integrity of the dosage form changes over time and in response to environmental factors like temperature and humidity. In this context, QF-PLGA-NPs and QF-PLGA-ISG NPs were kept under accelerated conditions for 3 months while being stored at 4 °C. QF formulations were discovered to exhibit negligible alterations in PS, PDI, and zeta and %EE, demonstrating that developed formulations maintained their integrity throughout storage [32].

Subsequently, the safety of the QF-PLGA-ISG on nasal epithelial cells is crucial to demonstrating nasal mucosa's vitality after chronic treatments. Therefore, the safety of QF-PLGA-ISG and Blank PLGA-ISG were assessed against normal nasal epithelial cell lines, RPMI-2650. The findings of this study demonstrated the blank formulation did not cause any cytotoxicity throughout 24 h of treatment. Even the QF-PLGA-ISG was non-toxic against RPMI-2650 after 24 h of exposure. Overall, the outcomes of the present study demonstrate the safety potential of QF-PLGA-ISG for IN delivery against brain disorders [48,53].

Improved intracellular uptake/penetration of drug-loaded formulations is crucial for therapeutic efficacy. The physicochemical concerns, such as particle size, shape, surface charge, and therapeutic solubility of optimized formulation, are critical to achieving efficient cellular permeation/uptake. As reported previously [65], nanoformulation with a size <200 nm is excellent for improving intracellular uptake while being small sufficiently to avoid mucociliary clearance and enzymatic degradation. The *in-vitro* cellular uptake, both qualitative and quantitative, was estimated through fluorescence microscopy and Nexcelom Cellometer Vision. In contrast, the C6-PLGA-ISG formulation displayed superior intracellular uptake in RPMI-2650 cell lines compared to plain coumarin-6. The outcomes of fluorescence microscopy demonstrated that C6-PLGA-ISG localized in the cells for a prolonged time with maximum fluorescence intensity. The results confirmed the highest uptake for formulation due to the cationic particles, *i.e.*, CH-P407, which highlights the sustained release prospect of PLGA ISG in intracellular environments. Later, the cell uptake by Cellometer Vision reflects that the C6-PLGS-ISG formulation treated cells exhibit excellent fluorescence intensity, which was more magnificent than the fluorescence intensities of the C6 solution. Such outcomes occurred due to the interaction of the cationic charge of PLGA-ISG with the anionic surface of the cell membrane. That helped to facilitate the absorption of the formulation into the cells. Hence, CH-P407, as a cationic compound, improved the cellular uptake and drug permeation. The C6-PLGA-ISG formulation with a significant positive charge *(+20.5 mV)* demonstrated an

excessive uptake profile, which could help protect the formulation from ciliary clearance and enzymatic degradation [47,51].

A permeation study confirmed improved QF permeation across nasal cell line monolayer. As reported, charge modification is relevant for opening tight junctions of the barrier, enhancing the permeation of medicines towards the site of action. This may be because the mucus layer is widely known to alter particle dispersion and drug permeability across mucosal tissues. Positively charged formulations are frequently retained in the mucus network because polyanionic mucin glycoproteins, mainly, are the major proteins involved in contact filtering. The RPMI-2650 cells were grown for 16 days to prepare nasal epithelial monolayer in an air-liquid interface. As previously reported [53], the developed membrane represented the human nasal mucosa. In this work, cationic QF-PLGA-ISG demonstrated enhanced cellular permeation compared to the QF. Therefore, CH-P407 coated cationic PLGA-ISG formulation can permeate across barriers. The findings of the permeability investigation showed that QF-PLGA-ISG might avoid mucociliary clearance (reflux mechanism of nasal physiology) and help to permeate QF across the membrane safely [48]. These outcomes demonstrate the potential of the developed formulation to enhance QF penetration towards the CNS by circumventing the BBB. Finally, outcomes from the current investigation demonstrate a definite potential of QF-PLGA-ISG for nose-to-brain delivery in mental disorders, schizophrenia.

Permeation outcomes across EpiNasal™ tissue samples demonstrated the potency of QF-PLGA-ISG formulation in QF permeation. The EpiNasal™ tissue permeation results strongly supported the findings of permeation across RPMI-2650 nasal epithelial cell monolayer. Many researchers have corroborated *in-vitro* permeation data with *in-vivo* bioavailability studies and have reported strong *in-vitro in-vivo* correlation. Inoue et al., 2020, [66] obtained a significant correlation between *in-vitro* Calu-3 cell permeability and rats nasal permeation rate, indicating that nasal drug permeability and bioavailability strongly correlate with *in-vitro* permeability. Similarly, Leonard et al., 2007, [67] performed *an in-vitro and in-vivo* correlation for IN formulation, and the results confirmed improved drug bioavailability with an *in-vitro* and *in-vivo* correlation. Currently, Nozohouri et al., 2022, [68] also found a strong correlation between *in-vitro* and *in-vivo* permeability data for CNS-acting formulations. All the findings from earlier investigations strongly supported that the *in-vitro* studies correlate with *in-vivo* studies. Furthermore, the results of permeation across RPMI-2650 cells monolayer and EpiNasal™ discovered similar, which could support and encourage the *in-vivo* studies. These advantageous outcomes documented the penetrating potential of developed QF-PLGA-ISG towards the CNS by circumventing the BBB. Additionally, histopathological screenings confirmed the safety of developed formulations against EpiNasal™ tissues. Hence, according to the observations of the overall investigation, the developed formulation was found safe and effective for the proposed treatment. Finally, outcomes from the current research demonstrate a definite potential of QF-PLGA-ISG for nose-to-brain delivery in mental disorders, schizophrenia.

5. Conclusions

Current work focused on increasing QF intranasal permeability and physicochemical stability to improve absorption and biological effectiveness in mental disorders. A noninvasive strategy for IN drug delivery for QF, an antipsychotic agent, was developed by formulation of ISG using ionic and thermo-responsive polymers. It was discovered that this cutting-edge method of drug administration could avoid BBB interactions and deliver QF directly to the brain. Biodegradable PLGA-ISG has the potential to reduce QF dose, dosing frequency, and associated toxicities, enabling effective delivery of QF to the CNS *via* the IN route. In addition, the *in-vitro* release study of QF-PLGA-ISG reflected sustained drug release in SNES over 24 h, which could assess the prolonged delivery of QF to the brain. *Ex-vivo* hemocompatibility confirmed that the developed formulation does not cause signs of hemolysis compared to pure QF and negative control. In addition, *in-vitro* cytotoxicity studies proved the safety of QF-PLGA-ISG than pure QF against RPMI-2650 human nasal epithelial cells. Transwell™ permeability studies showed that reducing nasal clearance due to mucoadhesive agents and flux could improve drug transport across the nasal epithelium, thereby increasing the permeability of drug across RPMI-2650 cells in presence of biodegradable PLGA-polymer. Simultaneously, EpiNasal tissue permeability studies strongly correlated with the permeability of RPMI-2650 cell monolayers. EpiNasal tissue permeation studies revealed the potential of the QF-PLGA-ISG formulation to cross the nasal tissue barrier, which strongly reinforces that the developed IN formulation has great potential for treating CNS disorders. Finally, the histological reports demonstrated no significant damage in treated EpiNasal™ tissues, which confirmed the safety of optimized QF-PLGA-ISG formulation in IN application. Therefore, the PLGA-ISG delivery of antipsychotics has been successfully projected towards the CSN, with an excellent future for safe and economical therapy of schizophrenia.

Funding

This work was supported with research funds of VG by the College of Pharmacy and Health Sciences, St. John's University, Queens, New York, USA, DGG and MG were supported by an industry grant to VG. AU, and MQ were supported by the teaching assistantships from the College of Pharmacy & Health Sciences, St. John's University, Queens, New York, USA.

CRediT authorship contribution statement

Dnyandev G. Gadhave: Conceptualization, Data curation, Formal analysis, Investigation, Methodology, Software, Validation, Writing – original draft. **Mural Quadros:** Investigation, Methodology. **Akanksha R. Ugale:** Investigation, Methodology. **Mimansa Goyal:** Investigation, Methodology. **Seyoum Ayehunie:** Funding acquisition, Resources. **Vivek Gupta:** Conceptualization, Funding acquisition, Methodology, Project administration, Resources, Supervision, Writing – review & editing.

Declaration of competing interest

The authors declare that they have no known financial conflicts that may have looked to have influenced the research presented in this study.

Data availability

Data will be made available on request.

Appendix A. Supplementary data

Supplementary data to this article can be found online at https://doi.org/10.1016/j.ijbiomac.2024.131491.

References

[1] D. Gadhave, S. Tupe, A. Tagalpallewar, B. Gorain, H. Choudhury, C. Kokare, Nose-to-brain delivery of amisulpride-loaded lipid-based poloxamer-gellan gum nanoemulgel: in vitro and in vivo pharmacological studies, Int. J. Pharm. 607 (2021) 121050, https://doi.org/10.1016/j.ijpharm.2021.121050.
[2] U. Seju, A. Kumar, K.K. Sawant, Development and evaluation of olanzapine-loaded PLGA nanoparticles for nose-to-brain delivery: in vitro and in vivo studies, Acta Biomater. 7 (2011) 4169–4176, https://doi.org/10.1016/j.actbio.2011.07.025.
[3] D. Gadhave, A. Gupta, S. Khot, A. Tagalpallewar, C. Kokare, Nose-to-brain delivery of paliperidone palmitate poloxamer-guar gum nanogel: formulation, optimization and pharmacological studies in rats, Ann. Pharm. Fr. 81 (2023) 315–333, https://doi.org/10.1016/j.pharma.2022.08.010.
[4] D.G. Gadhave, A.A. Tagalpallewar, C.R. Kokare, Agranulocytosis-protective olanzapine-loaded nanostructured lipid carriers engineered for CNS delivery:

optimization and hematological toxicity studies, AAPS PharmSciTech 20 (2019) 22, https://doi.org/10.1208/s12249-018-1213-y.
[5] Y. Qu, A. Li, L. Ma, S. Iqbal, X. Sun, W. Ma, C. Li, D. Zheng, Z. Xu, Z. Zhao, D. Ma, Nose-to-brain delivery of disulfiram nanoemulsion in situ gel formulation for glioblastoma targeting therapy, Int. J. Pharm. 597 (2021) 120250, https://doi.org/10.1016/j.ijpharm.2021.120250.
[6] C. Fornaguera, A. Dols-Perez, G. Calderó, M.J. García-Celma, J. Camarasa, C. Solans, PLGA nanoparticles prepared by nano-emulsion templating using low-energy methods as efficient nanocarriers for drug delivery across the blood–brain barrier, J. Control. Release 211 (2015) 134–143, https://doi.org/10.1016/j.jconrel.2015.06.002.
[7] D.G. Gadhave, V.V. Sugandhi, C.R. Kokare, Potential biomaterials and experimental animal models for inventing new drug delivery approaches in the neurodegenerative disorder: multiple sclerosis, Brain Res. 1822 (2024) 148674, https://doi.org/10.1016/j.brainres.2023.148674.
[8] J.S. Maan, M. Ershadi, I. Khan, A. Saadabadi, Quetiapine, in: StatPearls, StatPearls Publishing, Treasure Island (FL), 2024. http://www.ncbi.nlm.nih.gov/books/NBK459145/. (Accessed 21 March 2024).
[9] B. Shah, D. Khunt, M. Misra, H. Padh, Non-invasive intranasal delivery of quetiapine fumarate loaded microemulsion for brain targeting: formulation, physicochemical and pharmacokinetic consideration, Eur. J. Pharm. Sci. 91 (2016) 196–207, https://doi.org/10.1016/j.ejps.2016.05.008.
[10] C. Zhou, S. Xue, F. Xue, L. Liu, J. Liu, Q. Ma, J. Qin, Q. Tan, H. Wang, Z. Peng, The impact of quetiapine on the brain lipidome in a cuprizone-induced mouse model of schizophrenia, Biomed. Pharmacother. 131 (2020) 110707, https://doi.org/10.1016/j.biopha.2020.110707.
[11] K.-Y. Fan, W.-Y. Chen, M.-C. Huang, Quetiapine-associated leucopenia and thrombocytopenia: a case report, BMC Psychiatry 15 (2015) 110, https://doi.org/10.1186/s12888-015-0495-9.
[12] F.C. Arslan, D.S. Aykut, C. Ince, A. Tiryaki, Neutropenia and thrombocytopenia induced by quetiapine monotherapy: a case report and review of literature, Klinik Psikofarmakoloji Bülteni-bulletin of clinical, Psychopharmacology 26 (2016) 319–323, https://doi.org/10.5455/bcp.20151219072235.
[13] G. Crépeau-Gendron, S. L'Heureux, Quetiapine XR-induced neutropenia: is a clozapine trial still possible for treatment-resistant schizophrenia? A case report: Clozapine after quetiapine XR-induced neutropenia, Early Intervention in Psychiatry 9 (2015) 151–155, https://doi.org/10.1111/eip.12134.
[14] B. Ravi Shankar, Quetiapine-induced leucopenia and thrombocytopenia, Psychosomatics 48 (2007) 530–531, https://doi.org/10.1176/appi.psy.48.6.530.
[15] X. Li, M.D. Cameron, Potential role of a quetiapine metabolite in quetiapine-induced neutropenia and agranulocytosis, Chem. Res. Toxicol. 25 (2012) 1004–1011, https://doi.org/10.1021/tx2005635.
[16] D. Gadhave, S. Khot, S. Tupe, M. Shinde, A. Tagalpallewar, B. Gorain, C. Kokare, Nose-to-brain delivery of octreotide acetate in situ gel for pituitary adenoma: pharmacological and in vitro cytotoxicity studies, Int. J. Pharm. 629 (2022) 122372, https://doi.org/10.1016/j.ijpharm.2022.122372.
[17] S.A. Kumbhar, C.R. Kokare, B. Shrivastava, B. Gorain, H. Choudhury, Antipsychotic potential and safety profile of TPGS-based Mucoadhesive aripiprazole Nanoemulsion: development and optimization for nose-to-brain delivery, J. Pharm. Sci. 110 (2021) 1761–1778, https://doi.org/10.1016/j.xphs.2021.01.021.
[18] B. Shah, D. Khunt, M. Misra, Comparative evaluation of intranasally delivered quetiapine loaded mucoadhesive microemulsion and polymeric nanoparticles for brain targeting: pharmacokinetic and gamma scintigraphy studies, Futur J Pharm Sci 7 (2021) 6, https://doi.org/10.1186/s43094-020-00156-5.
[19] R. Pathak, R. Prasad Dash, M. Misra, M. Nivsarkar, Role of mucoadhesive polymers in enhancing delivery of nimodipine microemulsion to brain via intranasal route, Acta Pharm. Sin. B 4 (2014) 151–160, https://doi.org/10.1016/j.apsb.2014.02.002.
[20] F.A. Bruinsmann, A. De Cristo Soares Alves, A. De Fraga Dias, L.F. Lopes Silva, F. Visioli, A. Raffin Pohlmann, F. Figueiró, F. Sonvico, S. Stanisçuaski Guterres, Nose-to-brain delivery of simvastatin mediated by chitosan-coated lipid-core nanocapsules allows for the treatment of glioblastoma in vivo, Int. J. Pharm. 616 (2022) 121563, https://doi.org/10.1016/j.ijpharm.2022.121563.
[21] S. Cunha, M. Swedrowska, Y. Bellahnid, Z. Xu, J.M. Sousa Lobo, B. Forbes, A. C. Silva, Thermosensitive in situ hydrogels of rivastigmine-loaded lipid-based nanosystems for nose-to-brain delivery: characterisation, biocompatibility, and drug deposition studies, Int. J. Pharm. 620 (2022) 121720, https://doi.org/10.1016/j.ijpharm.2022.121720.
[22] D. Gadhave, B. Gorain, A. Tagalpallewar, C. Kokare, Intranasal teriflunomide microemulsion: an improved chemotherapeutic approach in glioblastoma, Journal of Drug Delivery Science and Technology 51 (2019) 276–289, https://doi.org/10.1016/j.jddst.2019.02.013.
[23] W.A. Banks, Drug delivery to the brain in Alzheimer's disease: consideration of the blood–brain barrier, Adv. Drug Deliv. Rev. 64 (2012) 629–639, https://doi.org/10.1016/j.addr.2011.12.005.
[24] S. Bhavna, M. Md, R. Ali, A. Ali, S. Bhatnagar, J. Baboota, Ali, donepezil nanosuspension intended for nose to brain targeting: in vitro and in vivo safety evaluation, Int. J. Biol. Macromol. 67 (2014) 418–425, https://doi.org/10.1016/j.ijbiomac.2014.03.022.
[25] Y. Yu, R. Feng, S. Yu, J. Li, Y. Wang, Y. Song, X. Yang, W. Pan, S. Li, Nanostructured lipid carrier-based pH and temperature dual-responsive hydrogel composed of carboxymethyl chitosan and poloxamer for drug delivery, Int. J. Biol. Macromol. 114 (2018) 462–469, https://doi.org/10.1016/j.ijbiomac.2018.03.117.
[26] S. Raman, A.A. Khan, S. Mahmood, Nose to brain delivery of selegiline loaded PLGA/lipid nanoparticles: synthesis, characterisation and brain pharmacokinetics evaluation, Journal of Drug Delivery Science and Technology 77 (2022) 103923, https://doi.org/10.1016/j.jddst.2022.103923.
[27] N. Ahmad, Rasagiline-encapsulated chitosan-coated PLGA nanoparticles targeted to the brain in the treatment of parkinson's disease, J. Liq. Chromatogr. Relat. Technol. 40 (2017) 677–690, https://doi.org/10.1080/10826076.2017.1343735.
[28] X. Wang, D. Gadhave, G. Chauhan, V. Gupta, Development and characterization of inhaled nintedanib-loaded PLGA nanoparticles using scalable high-pressure homogenization technique, Journal of Drug Delivery Science and Technology (2023) 105233, https://doi.org/10.1016/j.jddst.2023.105233.
[29] G.-F. Tong, N. Qin, L.-W. Sun, Development and evaluation of Desvenlafaxine loaded PLGA-chitosan nanoparticles for brain delivery, Saudi Pharmaceutical Journal 25 (2017) 844–851, https://doi.org/10.1016/j.jsps.2016.12.003.
[30] S. Ahmad, I. Khan, J. Pandit, N.A. Emad, S. Bano, K.I. Dar, M.M.A. Rizvi, M. D. Ansari, Mohd. Aqil, Y. Sultana, Brain targeted delivery of carmustine using chitosan coated nanoparticles via nasal route for glioblastoma treatment, Int. J. Biol. Macromol. 221 (2022) 435–445, https://doi.org/10.1016/j.ijbiomac.2022.08.210.
[31] B. Vaidya, V. Parvathaneni, N.S. Kulkarni, S.K. Shukla, J.K. Damon, A. Sarode, D. Kanabar, J.V. Garcia, S. Mitragotri, A. Muth, V. Gupta, Cyclodextrin modified erlotinib loaded PLGA nanoparticles for improved therapeutic efficacy against non-small cell lung cancer, Int. J. Biol. Macromol. 122 (2019) 338–347, https://doi.org/10.1016/j.ijbiomac.2018.10.181.
[32] R.S. Elbatanony, V. Parvathaneni, N.S. Kulkarni, S.K. Shukla, G. Chauhan, N. K. Kunda, V. Gupta, Afatinib-loaded inhalable PLGA nanoparticles for localized therapy of non-small cell lung cancer (NSCLC)—development and in-vitro efficacy, Drug Deliv. and Transl. Res. 11 (2021) 927–943, https://doi.org/10.1007/s13346-020-00802-8.
[33] N. Ahmad, R. Ahmad, F.J. Ahmad, W. Ahmad, M.A. Alam, M. Amir, A. Ali, Poloxamer-chitosan-based Naringenin nanoformulation used in brain targeting for the treatment of cerebral ischemia, Saudi Journal of Biological Sciences 27 (2020) 500–517, https://doi.org/10.1016/j.sjbs.2019.11.008.
[34] P.K. Sharma, M.K. Chauhan, Optimization and characterization of Brimonidine tartrate nanoparticles-loaded in situ gel for the treatment of Glaucoma, Curr. Eye Res. 46 (2021) 1703–1716, https://doi.org/10.1080/02713683.2021.1916037.
[35] D. Gadhave, N. Rasal, R. Sonawane, M. Sekar, C. Kokare, Nose-to-brain delivery of teriflunomide-loaded lipid-based carbopol-gellan gum nanogel for glioma: pharmacological and in vitro cytotoxicity studies, Int. J. Biol. Macromol. 167 (2021) 906–920, https://doi.org/10.1016/j.ijbiomac.2020.11.047.
[36] V. Parvathaneni, M. Goyal, N.S. Kulkarni, S.K. Shukla, V. Gupta, Nanotechnology based repositioning of an anti-viral drug for non-small cell lung Cancer (NSCLC), Pharm. Res. 37 (2020) 123, https://doi.org/10.1007/s11095-020-02848-2.
[37] V. Parvathaneni, N.S. Kulkarni, G. Chauhan, S.K. Shukla, R. Elbatanony, B. Patel, N.K. Kunda, A. Muth, V. Gupta, Development of pharmaceutically scalable inhaled anti-cancer nanotherapy – repurposing amodiaquine for non-small cell lung cancer (NSCLC), Mater. Sci. Eng. C 115 (2020) 111139, https://doi.org/10.1016/j.msec.2020.111139.
[38] V. Parvathaneni, S.K. Shukla, N.S. Kulkarni, V. Gupta, Development and characterization of inhalable transferrin functionalized amodiaquine nanoparticles – efficacy in non-small cell lung Cancer (NSCLC) treatment, Int. J. Pharm. 608 (2021) 121038, https://doi.org/10.1016/j.ijpharm.2021.121038.
[39] S.A. Kumbhar, C.R. Kokare, B. Shrivastava, B. Gorain, H. Choudhury, Preparation, characterization, and optimization of asenapine maleate mucoadhesive nanoemulsion using box-Behnken design: in vitro and in vivo studies for brain targeting, Int. J. Pharm. 586 (2020) 119499, https://doi.org/10.1016/j.ijpharm.2020.119499.
[40] A.-T. Chatzitaki, S. Jesus, C. Karavasili, D. Andreadis, D.G. Fatouros, O. Borges, Chitosan-coated PLGA nanoparticles for the nasal delivery of ropinirole hydrochloride: in vitro and ex vivo evaluation of efficacy and safety, Int. J. Pharm. 589 (2020) 119776, https://doi.org/10.1016/j.ijpharm.2020.119776.
[41] D. Gadhave, H. Choudhury, C. Kokare, Neutropenia and leukopenia protective intranasal olanzapine-loaded lipid-based nanocarriers engineered for brain delivery, Appl. Nanosci. 9 (2019) 151–168, https://doi.org/10.1007/s13204-018-0909-3.
[42] D.G. Gadhave, C.R. Kokare, Nanostructured lipid carriers engineered for intranasal delivery of teriflunomide in multiple sclerosis: optimization and *in vivo* studies, Drug Dev. Ind. Pharm. 45 (2019) 839–851, https://doi.org/10.1080/03639045.2019.1576724.
[43] S.K. Shukla, A. Chan, V. Parvathaneni, V. Gupta, Metformin-loaded chitosomes for treatment of malignant pleural mesothelioma – a rare thoracic cancer, Int. J. Biol. Macromol. 160 (2020) 128–141, https://doi.org/10.1016/j.ijbiomac.2020.05.146.
[44] H. Van De Ven, C. Paulussen, P.B. Feijens, A. Matheeussen, P. Rombaut, P. Kayaert, G. Van Den Mooter, W. Weyenberg, P. Cos, L. Maes, A. Ludwig, PLGA nanoparticles and nanosuspensions with amphotericin B: Potent in vitro and in vivo alternatives to Fungizone and AmBisome, J. Control. Release 161 (2012) 795–803. doi:https://doi.org/10.1016/j.jconrel.2012.05.037.
[45] G. Jeswani, L. Chablani, U. Gupta, R.K. Sahoo, K.T. Nakhate, Ajazuddin, development and optimization of paclitaxel loaded Eudragit/PLGA nanoparticles by simplex lattice mixture design: exploration of improved hemocompatibility and in vivo kinetics, Biomed. Pharmacother. 144 (2021) 112286, https://doi.org/10.1016/j.biopha.2021.112286.
[46] S. Godara, V. Lather, S.V. Kirthanashri, R. Awasthi, D. Pandita, Lipid-PLGA hybrid nanoparticles of paclitaxel: preparation, characterization, in vitro and in vivo evaluation, Mater. Sci. Eng. C 109 (2020) 110576, https://doi.org/10.1016/j.msec.2019.110576.
[47] X. Wang, V. Parvathaneni, S.K. Shukla, N.S. Kulkarni, A. Muth, N.K. Kunda, V. Gupta, Inhalable resveratrol-cyclodextrin complex loaded biodegradable

nanoparticles for enhanced efficacy against non-small cell lung cancer, Int. J. Biol. Macromol. 164 (2020) 638–650, https://doi.org/10.1016/j.ijbiomac.2020.07.124.
[48] V.S.S. Gonçalves, A.A. Matias, J. Poejo, A.T. Serra, C.M.M. Duarte, Application of RPMI 2650 as a cell model to evaluate solid formulations for intranasal delivery of drugs, Int. J. Pharm. 515 (2016) 1–10, https://doi.org/10.1016/j.ijpharm.2016.09.086.
[49] M. Goyal, G. Tulsyan, D.D. Kanabar, T. Chavan, A. Muth, V. Gupta, Poly vinyl pyrrolidone (PVP) based inhaled delivery carriers for olaparib for non-small cell lung cancer (NSCLC) treatment, Journal of Drug Delivery Science and Technology 87 (2023) 104767, https://doi.org/10.1016/j.jddst.2023.104767.
[50] IJMS | Free Full-Text | Repurposing Bedaquiline for Effective Non-Small Cell Lung Cancer (NSCLC) Therapy as Inhalable Cyclodextrin-Based Molecular Inclusion Complexes, (n.d.). https: //www.mdpi.com/1422-0067/22/9/4783 (accessed October 17, 2023).
[51] B. Vaidya, N.S. Kulkarni, S.K. Shukla, V. Parvathaneni, G. Chauhan, J.K. Damon, A. Sarode, J.V. Garcia, N. Kunda, S. Mitragotri, V. Gupta, Development of inhalable quinacrine loaded bovine serum albumin modified cationic nanoparticles: repurposing quinacrine for lung cancer therapeutics, Int. J. Pharm. 577 (2020) 118995, https://doi.org/10.1016/j.ijpharm.2019.118995.
[52] S.K. Shukla, V. Nguyen, M. Goyal, V. Gupta, Cationically modified inhalable nintedanib niosomes: enhancing therapeutic activity against non-small-cell lung cancer, Nanomedicine 17 (2022) 935–958, https://doi.org/10.2217/nnm-2022-0045.
[53] G. Vaz, A. Clementino, E. Mitsou, E. Ferrari, F. Buttini, C. Sissa, A. Xenakis, F. Sonvico, C.L. Dora, In vitro evaluation of curcumin- and quercetin-loaded Nanoemulsions for intranasal administration: effect of surface charge and viscosity, Pharmaceutics 14 (2022) 194, https://doi.org/10.3390/pharmaceutics14010194.
[54] S. Ladel, P. Schlossbauer, J. Flamm, H. Luksch, B. Mizaikoff, K. Schindowski, Improved in vitro model for intranasal mucosal drug delivery: primary olfactory and respiratory epithelial cells compared with the permanent nasal cell line RPMI 2650, Pharmaceutics 11 (2019) 367, https://doi.org/10.3390/pharmaceutics11080367.
[55] H. Choudhury, N.F.B. Zakaria, P.A.B. Tilang, A.S. Tzeyung, M. Pandey, B. Chatterjee, N.A. Alhakamy, S.K. Bhattamishra, P. Kesharwani, B. Gorain, S. Md, Formulation development and evaluation of rotigotine mucoadhesive nanoemulsion for intranasal delivery, Journal of Drug Delivery Science and Technology 54 (2019) 101301, https://doi.org/10.1016/j.jddst.2019.101301.
[56] R. Rukmangathen, I.M. Yallamalli, P.R. Yalavarthi, Formulation and biopharmaceutical evaluation of risperidone-loaded chitosan nanoparticles for intranasal delivery, Drug Dev. Ind. Pharm. 45 (2019) 1342–1350, https://doi.org/10.1080/03639045.2019.1619759.
[57] V. Fryer, J. Billings, Low-dose quetiapine causing agranulocytosis and leucopenia in a patient with benign neutropenia: a case report, Cureus 12 (n.d.) e8505. doi: https://doi.org/10.7759/cureus.8505.
[58] H. Akel, I. Csóka, R. Ambrus, A. Bocsik, I. Gróf, M. Mészáros, A. Szecskó, G. Kozma, S. Veszelka, M.A. Deli, Z. Kónya, G. Katona, In vitro comparative study of solid lipid and PLGA nanoparticles designed to facilitate nose-to-brain delivery of insulin, Int. J. Mol. Sci. 22 (2021) 13258, https://doi.org/10.3390/ijms222413258.
[59] D. Sharma, D. Maheshwari, G. Philip, R. Rana, S. Bhatia, M. Singh, R. Gabrani, S. K. Sharma, J. Ali, R.K. Sharma, S. Dang, Formulation and optimization of polymeric nanoparticles for intranasal delivery of lorazepam using box-Behnken design, In Vitro and In Vivo Evaluation, Biomed Res Int 2014 (2014) 156010, https://doi.org/10.1155/2014/156010.
[60] C. Kokare, D. Koli, D. Gadhave, C. Mote, G. Khandekar, Efavirenz-loaded intranasal microemulsion for crossing blood-CNS interfaces in neuronal-AIDS: pharmacokinetic and in vivo safety evaluation, Pharm. Dev. Technol. 25 (2020) 28–39, https://doi.org/10.1080/10837450.2019.1659818.
[61] P. Shah, P. Dubey, B. Vyas, A. Kaul, A.K. Mishra, D. Chopra, P. Patel, Lamotrigine loaded PLGA nanoparticles intended for direct nose to brain delivery in epilepsy: pharmacokinetic, pharmacodynamic and scintigraphy study, Artificial Cells, Nanomedicine, and Biotechnology 49 (2021) 511–522, https://doi.org/10.1080/21691401.2021.1939709.
[62] R. Xu, J. Wang, J. Xu, X. Song, H. Huang, Y. Feng, C. Fu, Rhynchophylline loaded-mPEG-PLGA nanoparticles coated with Tween-80 for preliminary study in Alzheimer's disease, Int. J. Nanomedicine 15 (2020) 1149–1160, https://doi.org/10.2147/IJN.S236922.
[63] A. Arici, H. Altun, C. Acipayam, Quetiapine induced autoimmune hemolytic Anemia in a child patient: a case report, Clin Psychopharmacol Neurosci 16 (2018) 501–504, https://doi.org/10.9758/cpn.2018.16.4.501.
[64] D.S. Jain, A.N. Bajaj, R.B. Athawale, S.S. Shikhande, A. Pandey, P.N. Goel, R. P. Gude, S. Patil, P. Raut, Thermosensitive PLA based nanodispersion for targeting brain tumor via intranasal route, Mater. Sci. Eng. C 63 (2016) 411–421, https://doi.org/10.1016/j.msec.2016.03.015.
[65] Q. Liang, H. Xiang, X. Li, C. Luo, X. Ma, W. Zhao, J. Chen, Z. Tian, X. Li, X. Song, development of Rifapentine-loaded PLGA-based nanoparticles: in vitro characterisation and in vivo study in mice , IJN 15 (2020) 7491–7507. doi: https://doi.org/10.2147/IJN.S257758.
[66] D. Inoue, T. Furubayashi, A. Tanaka, T. Sakane, K. Sugano, Quantitative estimation of drug permeation through nasal mucosa using in vitro membrane permeability across Calu-3 cell layers for predicting in vivo bioavailability after intranasal administration to rats, Eur. J. Pharm. Biopharm. 149 (2020) 145–153, https://doi.org/10.1016/j.ejpb.2020.02.004.
[67] A.K. Leonard, A.P. Sileno, G.C. Brandt, C.A. Foerder, S.C. Quay, H.R. Costantino, In vitro formulation optimization of intranasal galantamine leading to enhanced bioavailability and reduced emetic response in vivo, Int. J. Pharm. 335 (2007) 138–146, https://doi.org/10.1016/j.ijpharm.2006.11.013.
[68] S. Nozohouri, S.H. Esfahani, B. Noorani, D. Patel, H. Villalba, Y. Ghanwatkar, M. S. Rahman, Y. Zhang, U. Bickel, P.C. Trippier, V.T. Karamyan, T.J. Abbruscato, In-vivo and ex-vivo brain uptake studies of Peptidomimetic Neurolysin activators in healthy and stroke animals, Pharm. Res. 39 (2022) 1587–1598, https://doi.org/10.1007/s11095-022-03218-w.